

Embracing Heteroscedasticity for Probabilistic Time Series Forecasting

Yijun Wang¹ Qiyuan Zhuang¹ Xiu-Shen Wei¹

Abstract

Probabilistic time series forecasting (PTSF) aims to model the full predictive distribution of future observations, enabling both accurate forecasting and principled uncertainty quantification. A central requirement of PTSF is to embrace heteroscedasticity, as real-world time series exhibit time-varying conditional variances induced by nonstationary dynamics, regime changes, and evolving external conditions. However, most existing non-autoregressive generative approaches to PTSF, such as TimeVAE and K^2 VAE, rely on MSE-based training objectives that implicitly impose a homoscedastic assumption, thereby fundamentally limiting their ability to model temporal heteroscedasticity. To address this limitation, we propose the Location-Scale Gaussian VAE (LSG-VAE), a simple but effective framework that explicitly parameterizes both the predictive mean and time-dependent variance through a location-scale likelihood formulation. This design enables LSG-VAE to faithfully capture heteroscedastic aleatoric uncertainty and introduces an adaptive attenuation mechanism that automatically down-weights highly volatile observations during training, leading to improved robustness in trend prediction. Extensive experiments on nine benchmark datasets demonstrate that LSG-VAE consistently outperforms fifteen strong generative baselines while maintaining high computational efficiency suitable for real-time deployment.

1 Introduction

In recent years, deep learning has driven a paradigm shift in time series analysis (Lim & Zohren, 2021; Kong et al., 2025), achieving substantial progress in tasks ranging from imputation (Cao et al., 2018; Tashiro et al., 2021; Gao et al., 2025; Wang et al., 2025; 2024b) to anomaly detection (Xu

¹Department of Computer Science, Southeast University, Nanjing, China. Correspondence to: Xiu-Shen Wei <weixs@seu.edu.cn>.

Preprint. March 26, 2026.

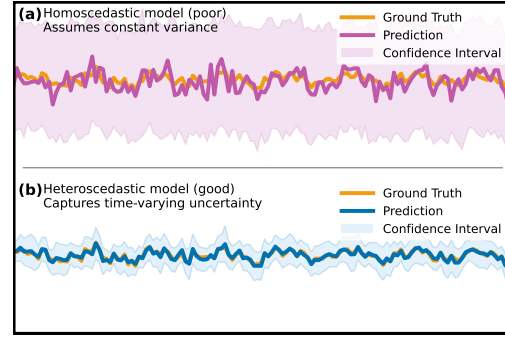


Figure 1. Homoscedastic vs. Heteroscedastic Forecasting. (a) Standard MSE-based models assume constant variance, leading the mean predictor to fit transient fluctuations. (b) LSG-VAE models time-varying uncertainty, allowing the mean prediction to focus on the underlying trend.

et al., 2022; Wang et al., 2023; Liu & Paparrizos, 2024; Miao et al., 2025; Wu et al., 2025b). Among these, Probabilistic Time Series Forecasting (PTSF) stands out as a critical capability for high-stakes decision-making (Gneiting & Raftery, 2007; Gneiting et al., 2007). In energy grids, probabilistic load forecasting is essential for risk-aware dispatch (Hong & Fan, 2016; Wang et al., 2024a; Sun et al., 2022); in quantitative finance and supply chains, accurate uncertainty modeling supports robust risk control under volatility (Sezer et al., 2020; Li et al., 2018; Huang et al., 2022). Unlike deterministic forecasters that yield only point estimates, PTSF aims to model the full predictive distribution, allowing for the precise evaluation of confidence intervals and tail risks (Zhang et al., 2024).

Despite the growing interest, capturing the intrinsic heteroscedasticity of real-world time series, characterized by conditional variances that fluctuate dynamically over time, remains a formidable challenge (Gneiting & Raftery, 2007). For instance, wind power generation exhibits stable patterns during calm weather but undergoes violent fluctuations during storms; similarly, financial markets alternate between periods of tranquility and bursts of extreme volatility during crises. A critical theoretical oversight persists in prevalent non-autoregressive generative forecasting paradigms, such as standard VAEs (Kingma & Welling, 2014; Desai et al., 2021) and K^2 VAE (Wu et al., 2025a): they predominantly rely on the Mean Squared Error (MSE) objective. Mathematically, minimizing MSE imposes a rigid homoscedastic assumption ($\sigma^2 = \text{const}$) (Kendall & Gal, 2017). This as-

sumption fundamentally mismatches the intrinsic nature of real-world data, which is characterized by dynamic, input-dependent volatility.

As illustrated in Figure 1(a), when confronted with volatile observations, such models lack an explicit mechanism to decouple the underlying trend from aleatoric uncertainty. Consequently, the MSE objective disproportionately penalizes high-variance fluctuations, rendering the mean predictor susceptible to overfitting these stochastic deviations and resulting in degraded generalization.

To address these limitations, we advocate a simple but effective philosophy: the difficulty often lies not in modeling increasingly complex latent dynamics, but in the lack of explicit mechanisms to decouple underlying trends from transient volatility. Rather than introducing computationally heavy iterative generative procedures or relying on rigid MSE-based objectives, we ask: *Can a lightweight generative model be explicitly empowered to know when to be uncertain?*

Motivated by this intuition, we propose the Location-Scale Gaussian Variational Autoencoder (LSG-VAE). LSG-VAE bridges the gap between efficiency and probabilistic rigor. It adopts a non-autoregressive formulation to avoid error accumulation, while replacing the MSE surrogate with a principled location-scale likelihood. This formulation naturally induces an adaptive attenuation effect (visualized in Figure 1(b)). By dynamically estimating a time-dependent variance σ_t , the model yields confidence intervals with time-varying widths. From an optimization perspective, this corresponds to down-weighting the contribution of high-variance observations ($\propto 1/\sigma_t^2$) in the loss function. As a result, the scale component captures irreducible stochastic uncertainty, allowing the location component to remain stable and recover the underlying trend without being dominated by outliers.

In summary, LSG-VAE provides a streamlined framework for efficient and robust probabilistic forecasting. By employing a global latent dynamics module, the model captures long-term dependencies in a single forward pass, avoiding the recursive pitfalls of autoregressive architectures. Compared to diffusion-based approaches that rely on expensive iterative denoising (Rasul et al., 2021a; Shen & Kwok, 2023; Ye et al., 2025), LSG-VAE achieves substantially faster inference while maintaining competitive predictive uncertainty modeling. The main contributions of this work are as follows:

- **Unified Non-autoregressive Framework:** We propose LSG-VAE, a streamlined framework that integrates a location-scale likelihood into a non-autoregressive architecture. This design not only circumvents the error accumulation of autoregressive

models but also introduces an intrinsic adaptive attenuation mechanism, enabling the model to dynamically down-weight high-variance observations and robustly decouple underlying trends from irreducible uncertainty.

- **Universality of the LSG Paradigm:** We validate that our proposed heteroscedastic modeling principle is model-agnostic and transferable. By extending the LSG mechanism to other generative backbones, such as GAN-based (TimeGAN) and Koopman-based (K^2 VAE) models, we demonstrate that this simple but effective philosophy consistently enhances probabilistic forecasting performance across diverse architectures.
- **Strong Performance and Efficiency:** Extensive experiments on 9 real-world benchmarks demonstrate that LSG-VAE consistently outperforms a wide range of strong baselines in both predictive accuracy and uncertainty calibration, while achieving significantly lower inference latency. We release our code at <https://anonymous.4open.science/r/LSG-VAE>.

2 Methodology

2.1 Problem Formulation and Motivation

2.1.1 PROBABILISTIC FORECASTING FORMULATION

We consider a multivariate time series forecasting scenario. Let $\mathcal{X} = \{\mathbf{x}_t\}_{t=1}^L$ denote the historical look-back window of length L , where $\mathbf{x}_t \in \mathbb{R}^C$ represents the observed values of C variables at time step t . The objective is to model the conditional probability density of the future horizon $\mathcal{Y} = \{\mathbf{x}_t\}_{t=L+1}^{L+H}$ of length H :

$$p_{\theta}(\mathcal{Y}|\mathcal{X}). \quad (1)$$

Unlike deterministic approaches that yield a single point estimate $\hat{\mathcal{Y}} \approx \mathbb{E}[\mathcal{Y}|\mathcal{X}]$ (often minimizing L_2 distance), our goal is to capture the full predictive distribution. This formulation is essential for quantifying the *aleatoric uncertainty* intrinsic to the data generation process, specifically the time-varying volatility (heteroscedasticity).

2.1.2 THE HOMOSCEDASTIC TRAP IN VANILLA VAES

The Variational Autoencoder (VAE) (Kingma & Welling, 2014) provides a powerful framework for this generative task by introducing a latent variable \mathbf{Z} . However, a critical limitation in prevalent time series VAEs is the implicit assumption of a *fixed-variance* Gaussian likelihood for the decoder:

$$p_{\theta}(\mathcal{X}|\mathbf{Z}) = \mathcal{N}(\mathcal{X}; \boldsymbol{\mu}_{\theta}(\mathbf{Z}), \sigma_{const}^2 \mathbf{I}). \quad (2)$$

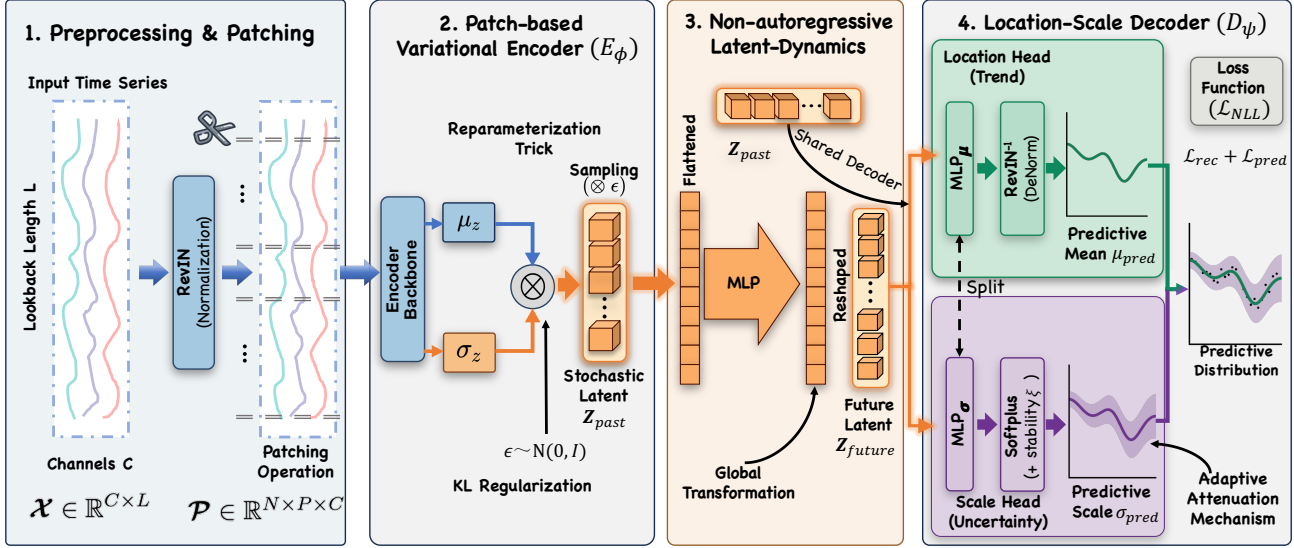


Figure 2. Overview of the LSG-VAE Framework. The model segments the input series into patches, encodes them into a probabilistic latent space, evolves the state via efficient global dynamics, and decodes the future using a dual-head mechanism to jointly predict location (μ) and scale (σ).

Under this assumption, maximizing the Evidence Lower Bound (ELBO) involves maximizing the log-likelihood term, which mathematically degenerates into the MSE objective:

$$\log p_{\theta}(\mathcal{X}|\mathbf{Z}) \propto - \sum_t \|\mathbf{x}_t - \boldsymbol{\mu}_t(\mathbf{Z})\|_2^2. \quad (3)$$

While computationally convenient, this derivation exposes a rigid homoscedastic inductive bias: the model implicitly assumes that uncertainty remains constant across time steps. Consequently, the vanilla VAE tends to behave similarly to a deterministic regressor, limiting its ability to represent time-varying uncertainty in real-world systems.

2.2 The LSG-VAE Framework

To overcome the limitations of the homoscedastic assumption, we present the Location-Scale Gaussian VAE (LSG-VAE), a generative framework designed to facilitate the modeling of global temporal dynamics separately from instantaneous local volatility. As depicted in Figure 2, the architecture is composed of three integral modules: (1) a *Patch-based Variational Encoder* responsible for extracting local semantic contexts; (2) a *Non-autoregressive Latent Dynamics* module that efficiently evolves the temporal state; and (3) a *Location-Scale Probabilistic Decoder* that parameterizes the final predictive distribution.

2.2.1 PATCHING AND VARIATIONAL ENCODING

To alleviate the computational bottlenecks of point-wise processing and to better capture local semantic structures, we employ a patching strategy (Nie et al., 2023). We first

apply Reversible Instance Normalization (RevIN) to the input \mathcal{X} to mitigate non-stationarity (Kim et al., 2022). The normalized series is then segmented into N non-overlapping patches $\mathcal{P} \in \mathbb{R}^{N \times P \times C}$, where P denotes the patch length.

The encoder E_{ϕ} maps these patches into a stochastic latent space. Following the variational autoencoder framework (Kingma & Welling, 2014), we model the posterior distribution of the past latent states \mathbf{Z}_{past} as a diagonal Gaussian to account for epistemic uncertainty arising from noisy observations:

$$q_{\phi}(\mathbf{Z}_{past} | \mathcal{P}) = \mathcal{N}(\boldsymbol{\mu}_z, \boldsymbol{\sigma}_z^2). \quad (4)$$

Here, $(\boldsymbol{\mu}_z, \boldsymbol{\sigma}_z) = E_{\phi}(\mathcal{P})$. Utilizing the reparameterization trick (Kingma & Welling, 2014), we sample $\mathbf{Z}_{past} = \boldsymbol{\mu}_z + \boldsymbol{\epsilon} \odot \boldsymbol{\sigma}_z$, where $\boldsymbol{\epsilon} \sim \mathcal{N}(0, \mathbf{I})$. This stochastic injection regularizes the latent representation and improves robustness to input perturbations.

2.2.2 NON-AUTOREGRESSIVE LATENT DYNAMICS

Modeling the transition from past latent representations \mathbf{Z}_{past} to future representations \mathbf{Z}_{future} is a critical component. While recurrent architectures (e.g., RNNs) are capable of sequential modeling, they are prone to error accumulation and suffer from high latency in long-horizon forecasting (Bengio et al., 2015). To address this limitation, we propose a lightweight Non-autoregressive Latent Dynamics mechanism.

We adopt the modeling assumption that the high-level semantic evolution of a time series can be approximated by a global transformation in the latent space. Specifically, we flatten the past latent representations and project them

directly to the future horizon:

$$\mathbf{Z}_{future} = \text{Projection}(\text{Flatten}(\mathbf{Z}_{past})) \in \mathbb{R}^{M \times D}, \quad (5)$$

where M denotes the number of future patches. This non-autoregressive design enables the model to capture global temporal dependencies and generate the entire future horizon in a single forward pass. This parallel decoding mechanism eliminates the computational bottleneck of recursive generation, resulting in improved computational efficiency compared to autoregressive probabilistic forecasters such as DeepAR (Salinas et al., 2020) and TimeGrad (Rasul et al., 2021a).

2.2.3 LOCATION-SCALE PROBABILISTIC DECODING

This module constitutes the core mechanism for capturing intrinsic heteroscedasticity. Conventional VAEs for time series typically utilize a single-head decoder, implicitly assuming a fixed-variance Gaussian likelihood. We contend that this assumption is often inadequate for real-world data exhibiting dynamic volatility. To address this limitation, we introduce a shared Dual-Head Decoder D_ψ . This decoder operates with identical weights on both the historical latent representations \mathbf{Z}_{past} and the future latent representations \mathbf{Z}_{future} , ensuring a consistent mapping from latent space to the observation space.

In terms of implementation, we do not employ two separate networks. Instead, we use a single MLP backbone to project the latent states. The output of this MLP is then split along the last dimension to decouple the location and scale parameters simultaneously. The first part of the split serves as the Location Head, capturing the central tendency (trend and seasonality). To restore the original scale of the data, the inverse RevIN operation is applied:

$$\boldsymbol{\mu} = \text{RevIN}^{-1}(\text{MLP}_\mu(\mathbf{Z})). \quad (6)$$

The second part constitutes the *Scale Head*, estimating the instantaneous volatility (aleatoric uncertainty). To ensure numerical stability and strictly positive standard deviations, we model the log-variance via a Softplus activation:

$$\boldsymbol{\sigma} = \text{Softplus}(\text{MLP}_\sigma(\mathbf{Z})) + \xi, \quad (7)$$

where ξ is a small stability constant (e.g., 10^{-6}). Crucially, this dual-head mechanism empowers the model to rigorously capture the residual uncertainty that remains unexplained by the location estimate in both historical and future contexts.

2.2.4 OBJECTIVE FUNCTION: EMBRACING HETEROSEDASTICITY

The training objective is to maximize the Evidence Lower Bound (ELBO). Unlike many forecasting-oriented VAE variants that rely on MSE-based reconstruction objectives,

we reformulate the objective to explicitly account for heteroscedasticity in both reconstruction and prediction phases.

The Composite Location-Scale Loss. We adopt the Gaussian Negative Log-Likelihood (NLL) for both the look-back window reconstruction (\mathcal{L}_{rec}) and the future horizon prediction (\mathcal{L}_{pred}). The total loss function \mathcal{L} is defined as:

$$\mathcal{L} = \underbrace{\mathcal{L}_{rec}(\mathcal{X})}_{\text{Reconstruction}} + \underbrace{\mathcal{L}_{pred}(\mathcal{Y})}_{\text{Prediction}} + \beta \cdot D_{KL}(q_\phi(\mathbf{Z}_{past} | \mathcal{P}) || \mathcal{N}(0, \mathbf{I})). \quad (8)$$

Both \mathcal{L}_{rec} and \mathcal{L}_{pred} are computed using the heteroscedastic Gaussian NLL. For a generic sequence \mathbf{u} of length T (where \mathbf{u} is \mathbf{x} or \mathbf{y}), the loss is:

$$\mathcal{L}_{NLL}(\mathbf{u}) = \frac{1}{TC} \sum_{t,c} \left(\log \sigma_{t,c} + \frac{(\mathbf{u}_{t,c} - \boldsymbol{\mu}_{t,c})^2}{2\sigma_{t,c}^2} \right). \quad (9)$$

By jointly minimizing \mathcal{L}_{rec} and \mathcal{L}_{pred} , the model is forced to learn a latent representation that is both descriptive of historical patterns and predictive of future dynamics.

Theoretical Analysis (Adaptive Attenuation). The gradient of the NLL term reveals an adaptive attenuation mechanism:

$$\nabla_{\boldsymbol{\mu}} \mathcal{L}_{NLL} \propto \frac{1}{\sigma^2} (\mathbf{u} - \boldsymbol{\mu}). \quad (10)$$

When the model encounters an outlier or high volatility in the history (reconstruction) or uncertain future regimes (prediction), it learns to increase σ . This effectively downweights the gradient contribution of that specific point ($\frac{1}{\sigma^2} \rightarrow 0$), preventing the Location Head from overfitting to transient stochastic fluctuations. This mechanism transforms the model from a passive curve fitter into an active risk estimator. For a rigorous mathematical derivation of the heteroscedastic ELBO and a formal proof of this attenuation mechanism, please refer to the detailed theoretical analysis in Appendix B.

3 Experiments on Synthetic Data

In real-world empirical studies, the true aleatoric uncertainty is inherently latent and unobservable, making it difficult to rigorously verify whether a model is capturing volatility dynamics or merely overfitting residual artifacts (Kendall & Gal, 2017). To address this, we validate the heteroscedastic modeling capability of LSG-VAE within a controlled analytical environment where both the underlying trend and the volatility profile are mathematically defined and known (Gal & Ghahramani, 2016). This experiment serves as a critical verification of our Location–Scale formulation: the model must demonstrate the ability to disentangle the deterministic signal, modeled by the Location Head, from the time-varying volatility, captured by the Scale Head.

Data Generating Process We analyze univariate sequences governed by the process $y_t = \mu_t + \epsilon_t$, where the underlying deterministic trend is defined as $\mu_t = \sin(t)$ and the stochastic term follows $\epsilon_t \sim \mathcal{N}(0, \sigma_t^2)$. To stress-test the model under extreme heteroscedasticity, we introduce two distinct volatility profiles as illustrated in Figure 3. The first is a Regime-Switching scenario (Top Row), which simulates structural breaks by having σ_t alternate abruptly between stable (0.1) and high-volatility (1.0) states, thereby challenging the model’s adaptability to sudden distributional shifts. The second is a Periodic pattern (Bottom Row), defined by a continuous volatility trajectory $\sigma_t = 0.5 + 0.4 \cos(t)$; this profile is deliberately phase-shifted relative to the mean to rigorously test the model’s ability to decouple correlated but distinct dynamics.

Results and Analysis Figure 3 visualizes the forecasting and variance recovery performance, confirming LSG-VAE’s fidelity in reconstructing latent heteroscedastic dynamics. In the Regime-Switching scenario (a-b), the predicted scale $\hat{\sigma}_t$ tightly tracks the ground-truth step function with high correlation ($\rho = 0.985$). This precise estimation allows the confidence intervals to exhibit a distinct “breathing” behavior—instantly expanding during volatility spikes to encapsulate noise and contracting during stable periods—without distorting the trend prediction. Similarly, in the Periodic scenario (c-d), the model achieves near-perfect disentanglement ($\rho = 0.999$), effectively distinguishing the signal’s phase from the cyclic volatility profile. Crucially, these results demonstrate that the Location and Scale heads have successfully specialized in their respective roles, transforming the model from a passive curve fitter into an active risk estimator that separates what is predicted (trend) from what is uncertain (volatility).

4 Experiments on Real-World Data

We conduct extensive experiments to comprehensively evaluate the effectiveness, robustness, and generalizability of LSG-VAE. Our evaluation focuses on large-scale real-world probabilistic time series forecasting tasks, followed by ablation studies, qualitative analysis, generalization experiments, and efficiency comparisons.

To rigorously evaluate LSG-VAE against SOTA methods, we conduct extensive experiments under two established evaluation protocols. First, we follow the comprehensive benchmarking setting introduced in ProbTS (Zhang et al., 2024), which provides a unified framework for comparing both point and probabilistic time series forecasters under standard accuracy metrics (Zhang et al., 2024). In addition, we align this setting with recent VAE-based generative forecasting work, such as K^2 VAE, to ensure fair comparison across deterministic and probabilistic models (Wu et al., 2025a). Second, we adopt the experimental protocol com-

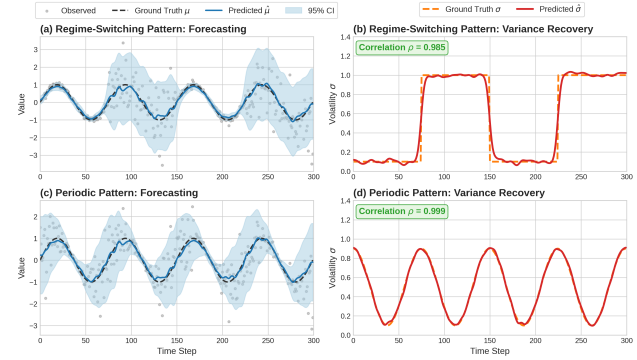


Figure 3. Qualitative results on synthetic datasets. Left: forecasting with adaptive 95% confidence intervals under varying volatility. Right: uncertainty recovery, where the predicted volatility $\hat{\sigma}_t$ closely matches the ground truth.

monly used by recent SOTA diffusion models for time series forecasting, which focuses on probabilistic calibration and distributional quality, as exemplified by NsDiff (Ye et al., 2025).

4.1 Evaluation under the K^2 VAE Protocol

Datasets We conduct experiments on nine widely-recognized real-world benchmarks from ProbTS (Zhang et al., 2024), spanning diverse domains: Energy (*ETTh1*, *ETTh2*, *ETTm1*, *ETTm2*, *Electricity*), Transportation (*Traffic*), Weather (*Weather*), Economics (*Exchange*), and Health (*ILI*). Following the standard protocol for long-term forecasting, we set the look-back window length to $L = 96$ for all datasets, except for *ILI* where $L = 36$. The forecasting horizons are set to $H \in \{96, 192, 336, 720\}$ for the general datasets and $H \in \{24, 36, 48, 60\}$ for *ILI*.

Baselines We compare LSG-VAE with 11 competitive baselines, covering both deterministic and probabilistic forecasting paradigms. Specifically, the selected baselines include deep point forecasters such as FITS (Xu et al., 2024), PatchTST (Nie et al., 2023), iTransformer (Liu et al., 2024), and Koopa (Liu et al., 2023), which are originally designed for deterministic prediction. For fair probabilistic evaluation, these models are augmented with a Gaussian output head to predict distribution parameters (μ, σ). In addition, we consider a broad range of probabilistic and generative models, including TSDiff (Kollovieh et al., 2023), TimeGrad (Rasul et al., 2021a), CSDI (Tashiro et al., 2021), GRU NVP, GRU MAF, Trans MAF (Rasul et al., 2021b), as well as K^2 VAE (Wu et al., 2025a). Implementation details are provided in Appendix C.4.

Metrics We employ two complementary metrics: Continuous Ranked Probability Score (CRPS) to measure the distributional fit and Normalized Mean Absolute Error (NMAE) to assess point prediction accuracy. Lower values indicate better performance for both metrics. Detailed descriptions

Embracing Heteroscedasticity for Probabilistic Time Series Forecasting

Table 1. Comparison on long-term probabilistic forecasting (forecasting horizon $L=720$) scenarios across nine real-world datasets. Lower CRPS or NMAE values indicate better predictions. The means and standard errors are based on 5 independent runs of retraining and evaluation. **Red**: the best, **Blue**: the 2nd best. The full results of all four horizons 96, 192, 336, 720 are listed in Table 6, 7 in Appendix C.5.

Model	Metric	ETM1	ETM2	ETTh1	ETTh2	Electricity	Traffic	Weather	Exchange	ILI
FITS	CRPS	0.305±0.024	0.449±0.034	0.348±0.025	0.314±0.022	0.115±0.024	0.374±0.004	0.267±0.003	0.074±0.011	0.211±0.011
	NMAE	0.406±0.072	0.540±0.052	0.468±0.012	0.401±0.022	0.149±0.012	0.453±0.022	0.317±0.021	0.097±0.011	0.245±0.017
PatchTST	CRPS	0.304±0.029	0.229±0.036	0.323±0.020	0.304±0.018	0.127±0.015	0.214±0.001	0.142±0.005	0.097±0.007	0.233±0.019
	NMAE	0.382±0.066	0.288±0.034	0.428±0.024	0.371±0.021	0.164±0.024	0.253±0.012	0.152±0.029	0.126±0.001	0.287±0.023
iTransformer	CRPS	0.455±0.021	0.311±0.024	0.350±0.019	0.542±0.015	0.109±0.044	0.284±0.004	0.133±0.004	0.087±0.023	0.222±0.020
	NMAE	0.490±0.038	0.385±0.042	0.449±0.022	0.667±0.012	0.140±0.009	0.361±0.030	0.147±0.019	0.113±0.015	0.278±0.017
KoopA	CRPS	0.295±0.027	0.233±0.025	0.318±0.009	0.293±0.026	0.113±0.018	0.358±0.022	0.140±0.007	0.091±0.012	0.228±0.022
	NMAE	0.377±0.037	0.290±0.033	0.412±0.008	0.286±0.042	0.149±0.025	0.432±0.032	0.162±0.009	0.116±0.022	0.288±0.031
TSDiff	CRPS	0.478±0.027	0.344±0.046	0.516±0.027	0.406±0.056	0.478±0.005	0.391±0.002	0.152±0.003	0.082±0.010	0.263±0.022
	NMAE	0.622±0.045	0.416±0.065	0.657±0.017	0.482±0.022	0.622±0.142	0.478±0.006	0.141±0.026	0.142±0.009	0.272±0.020
GRU NVP	CRPS	0.546±0.036	0.561±0.273	0.502±0.039	0.539±0.090	0.114±0.013	0.211±0.004	0.110±0.004	0.079±0.009	0.307±0.005
	NMAE	0.707±0.050	0.749±0.385	0.643±0.046	0.688±0.161	0.144±0.017	0.264±0.006	0.135±0.008	0.103±0.009	0.333±0.005
GRU MAF	CRPS	0.536±0.033	0.272±0.029	0.393±0.043	0.990±0.223	0.106±0.007	-	0.122±0.006	0.160±0.019	0.172±0.034
	NMAE	0.711±0.081	0.355±0.048	0.496±0.019	1.092±0.019	0.136±0.098	-	0.149±0.034	0.182±0.010	0.216±0.014
Trans MAF	CRPS	0.688±0.043	0.355±0.043	0.363±0.053	0.327±0.033	-	-	0.113±0.004	0.148±0.017	0.155±0.018
	NMAE	0.822±0.034	0.475±0.029	0.455±0.025	0.412±0.020	-	-	0.148±0.040	0.191±0.006	0.183±0.019
TimeGrad	CRPS	0.621±0.037	0.470±0.054	0.523±0.027	0.445±0.016	0.108±0.003	0.220±0.002	0.113±0.011	0.099±0.015	0.295±0.083
	NMAE	0.793±0.034	0.561±0.044	0.672±0.015	0.550±0.018	0.134±0.004	0.263±0.001	0.136±0.020	0.113±0.016	0.325±0.068
CSDI	CRPS	0.448±0.038	0.239±0.035	0.528±0.012	0.302±0.040	-	-	0.087±0.003	0.143±0.020	0.283±0.012
	NMAE	0.578±0.051	0.306±0.040	0.657±0.014	0.382±0.030	-	-	0.102±0.005	0.173±0.020	0.299±0.013
K^2 VAE	CRPS	0.294±0.026	0.221±0.023	0.314±0.011	0.280±0.014	0.087±0.005	0.200±0.001	0.084±0.003	0.069±0.005	0.142±0.008
	NMAE	0.373±0.032	0.275±0.035	0.396±0.012	0.278±0.020	0.117±0.019	0.248±0.010	0.099±0.009	0.084±0.017	0.167±0.017
LSG-VAE*	CRPS	0.279±0.020	0.166±0.018	0.310±0.012	0.174±0.010	0.080±0.006	0.192±0.003	0.073±0.003	0.065±0.004	0.130±0.005
	NMAE	0.367±0.023	0.207±0.026	0.389±0.013	0.223±0.015	0.111±0.012	0.236±0.009	0.086±0.006	0.077±0.012	0.155±0.006

* indicates that LSG-VAE significantly outperforms K^2 VAE under paired Wilcoxon signed-rank tests ($p < 0.05$).

of these metrics can be found in Appendix C.3.

Results and Analysis Table 1 summarizes the performance for the challenging long-term horizon ($H = 720$). A significant and counter-intuitive finding is that LSG-VAE consistently outperforms specialized point forecasters, such as PatchTST and iTransformer, even on the deterministic metric (NMAE). This empirically confirms that explicitly modeling heteroscedasticity enables the NLL objective to adaptively down-weight noisy samples, effectively robustifying the mean predictor against outliers. Furthermore, compared to the previous SOTA VAE-based method, K^2 VAE, our model achieves consistent improvements across all datasets. This highlights that the simple, principled Location-Scale paradigm offers a more effective approach for time series modeling than complex reconstruction schemes.

4.2 Evaluation under the NsDiff Protocol

Datasets To assess generative capability, we follow the specific protocol used in recent diffusion-based studies. We utilize 8 datasets: *ETT* (m1, m2, h1, h2), *Electricity*, *Traffic*, *Exchange*, and *ILI*. Consistent with this protocol, the input length is fixed at $L = 168$ (except ILI).

Baselines We compare against 6 advanced generative baselines, including the classic autoregressive diffusion model TimeGrad (Rasul et al., 2021a) and SOTA diffusion-based approaches, namely CSDI (Tashiro et al., 2021), TimeDiff (Shen & Kwok, 2023), DiffusionTS (Yuan & Qiao, 2024), TMDM (Li et al., 2024), and NsDiff (Ye et al., 2025).

Metrics In addition to CRPS, we employ the Quantile Interval Calibration Error (QICE) to strictly evaluate the calibration quality of the predicted confidence intervals. QICE measures the discrepancy between the empirical and nominal coverage probabilities, where a lower value indicates a more trustworthy uncertainty estimation. Detailed descriptions of these metrics can be found in Appendix C.3.

Results and Analysis As shown in Table 2, LSG-VAE demonstrates remarkable performance against competitive generative baselines. In terms of probabilistic performance, LSG-VAE achieves the best CRPS across all eight datasets, significantly outperforming recent SOTA diffusion models. This result is particularly notable given the efficiency gap: while diffusion-based approaches like CSDI and NsDiff require computationally expensive iterative denoising steps to reconstruct distributions, LSG-VAE achieves superior modeling quality in a single non-autoregressive forward pass. Furthermore, regarding calibration quality, LSG-VAE ranks either first or second in terms of QICE across the majority of datasets. This indicates that the confidence intervals generated by our Location-Scale decoder are not only accurate but also well-calibrated, faithfully reflecting the true aleatoric uncertainty of the data without the need for complex iterative refinement.

4.3 Ablation Studies

To thoroughly investigate the contribution of each component in our training objective, we conduct a component-wise ablation study. The total loss is defined as $\mathcal{L} =$

Embracing Heteroscedasticity for Probabilistic Time Series Forecasting

Table 2. Quantitative comparison of probabilistic forecasting on 8 real-world datasets ($L = 168, H = 192$). Metrics: CRPS and QICE (lower is better). **Red** indicates the best performance, and **Blue** indicates the 2nd best.

Model	Metric	ETM1	ETM2	ETTh1	ETTh2	Electricity	Traffic	Exchange	ILI
TimeGrad	CRPS	0.647	0.775	0.606	1.212	0.397	0.407	0.826	1.140
	QICE	6.693	6.962	6.731	9.488	7.118	4.581	9.464	6.519
CSDI	CRPS	0.524	0.817	0.492	0.647	0.577	1.418	0.855	1.244
	QICE	2.828	8.106	3.107	5.331	7.506	13.613	7.864	7.693
TimeDiff	CRPS	0.464	0.316	0.465	0.471	0.750	0.771	0.433	1.153
	QICE	14.795	13.385	14.931	14.813	15.466	15.439	14.556	14.942
DiffusionTS	CRPS	0.574	1.035	0.603	1.168	0.633	0.668	1.251	1.612
	QICE	5.605	9.959	6.423	9.577	8.205	5.958	10.411	10.090
TMDM	CRPS	0.375	0.289	0.452	0.383	0.461	0.557	0.336	0.967
	QICE	2.567	2.610	2.821	4.471	10.562	10.676	6.393	6.217
NsDiff	CRPS	<u>0.346</u>	<u>0.256</u>	<u>0.392</u>	<u>0.358</u>	<u>0.290</u>	<u>0.378</u>	<u>0.324</u>	<u>0.806</u>
	QICE	<u>2.041</u>	2.030	<u>1.470</u>	2.074	<u>6.685</u>	<u>3.601</u>	<u>5.930</u>	<u>5.598</u>
LSG-VAE	CRPS	0.236	0.130	0.288	0.174	0.080	0.190	0.032	0.107
	QICE	1.623	<u>2.373</u>	1.450	<u>2.385</u>	1.082	1.363	3.174	4.968

Table 3. Component-wise ablation on *ETTh1* and *Electricity*. We compare LSG-VAE with variants without prediction loss (w/o P), without reconstruction loss (w/o R), and a vanilla VAE (MSE). Metrics: CRPS and NMAE. **Bold** indicates the best result.

Dataset	Horizon	CRPS ↓				NMAE ↓			
		Van.	w/o P	w/o R	Ours	Van.	w/o P	w/o R	Ours
ETTh1	96	0.287	0.374	0.277	0.252	0.329	0.464	0.354	0.328
	192	0.323	0.378	0.282	0.277	0.368	0.470	0.370	0.365
	336	0.352	0.386	0.305	0.300	0.388	0.486	0.395	0.384
	720	0.355	0.393	0.318	0.310	0.396	0.504	0.398	0.389
Electricity	96	0.363	0.259	0.082	0.069	0.362	0.363	0.107	0.089
	192	0.363	0.261	0.086	0.075	0.364	0.363	0.112	0.096
	336	0.364	0.264	0.099	0.078	0.364	0.366	0.129	0.102
	720	0.370	0.269	0.103	0.080	0.370	0.371	0.135	0.111

$\mathcal{L}_{rec} + \mathcal{L}_{pred} + \beta D_{KL}$. We measure performance using CRPS (probabilistic calibration) and NMAE (deterministic accuracy). We compare the full LSG-VAE against three distinct variants: w/o Prediction ($\mathcal{L}_{pred} = 0$), which is trained exclusively on reconstructing historical patches to test whether latent dynamics can be learned without future supervision; w/o Reconstruction ($\mathcal{L}_{rec} = 0$), which removes the historical reconstruction loss to verify if the auxiliary reconstruction task aids in regularizing the latent space; and Vanilla VAE (MSE), which replaces the heteroscedastic Location-Scale NLL with a standard homoscedastic MSE loss.

The results on *ETTh1* and *Electricity*, summarized in Table 3, validate the synergy of our proposed components. First, the w/o Pred variant exhibits the sharpest deterioration in deterministic accuracy, confirming that explicit future supervision is indispensable for guiding the latent dynamics module. Similarly, the consistent performance drop in the w/o Rec variant indicates that historical reconstruction is essential for regularizing the latent space and preventing overfitting. Crucially, the Vanilla VAE significantly lags behind LSG-VAE in probabilistic metrics. This empirically proves that the homoscedastic bias inherent in the MSE objective severely limits uncertainty calibration, whereas our

Table 4. Generalizability analysis on *ETTh1* and *Weather* datasets ($L = 96, H = 96$). We compare the standard MSE-based baselines against our Location-Scale (LSG) variants. **Bold** indicates the better performance.

Model Framework	ETTh1		Weather	
	CRPS ↓	NMAE ↓	CRPS ↓	NMAE ↓
<i>Generative Adversarial Networks (GAN)</i>				
TimeGAN	0.277	0.347	0.106	0.117
LSG-GAN (Ours)	0.262	0.339	0.068	0.081
<i>Variational Autoencoders (VAE)</i>				
K^2 VAE	0.264	0.336	0.080	0.086
LSG- K^2 VAE (Ours)	0.251	0.332	0.065	0.076

Location-Scale formulation effectively captures dynamic volatility. Additionally, while we observe that LSG-VAE is robust to the KL divergence term, we retain it to ensure the theoretical integrity of the variational framework. Furthermore, we extend our investigation to architectural design choices. Detailed ablation studies concerning the impact of RevIN are provided in Appendix C.6. And hyperparameter sensitivity analysis can be found in the Appendix C.7.

4.4 Generalizability Analysis

A pivotal question remains: *Is the effectiveness of the Location-Scale objective limited to our specific architecture?* To demonstrate the universality of our heteroscedastic modeling paradigm, we extend the proposed principle to other generative frameworks.

Extension to GANs (LSG-GAN) To verify the generality of our approach beyond VAEs, we integrate the Location-Scale mechanism into the adversarial training framework. We construct LSG-GAN by modifying the classic TimeGAN architecture: the deterministic generator output is replaced with our dual-head parameterization, while the discriminator architecture remains unchanged. Crucially, the discriminator is trained to distinguish samples drawn

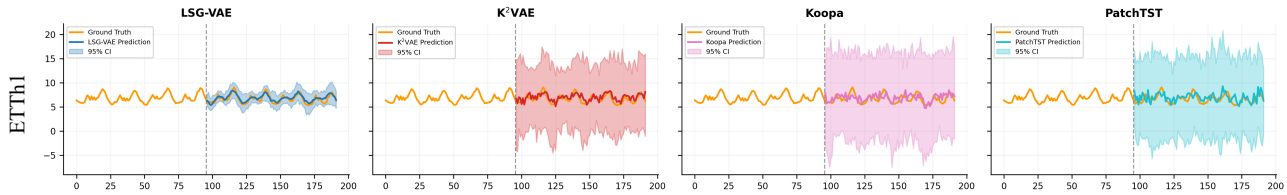


Figure 4. Visual comparison of probabilistic forecasting on *ETTh1*. All subfigures share a unified Y-axis scale. Additional visualization results are provided in Appendix C.8.

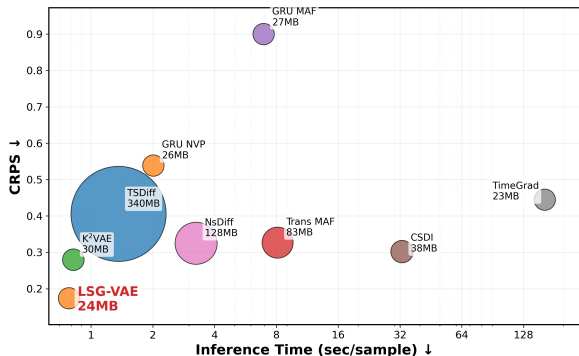


Figure 5. Efficiency vs. Performance comparison on *ETTh2* ($L = 96, H = 720$). The bubble size indicates inference memory usage (smaller is better).

from the predicted distribution $\mathcal{N}(\mu, \sigma^2)$ rather than deterministic point estimates, and the generator is supervised via the Gaussian NLL loss. As shown in Table 4 (Top), this simple modification consistently outperforms the MSE-based TimeGAN baseline on both *ETTh1* and *Weather* datasets. These results suggest that explicitly modeling heteroscedastic uncertainty provides complementary benefits to adversarial learning, enhancing distribution matching even in non-variational settings.

Enhancing SOTA VAEs (LSG- K^2 VAE) We further apply our paradigm to K^2 VAE, a SOTA method that originally relies on a deterministic reconstruction objective. By simply replacing its MSE reconstruction loss with our Location-Scale NLL objective—without any architectural changes to its core dynamics—we derive an enhanced variant termed LSG- K^2 VAE. Quantitative comparisons in Table 4 (Bottom) reveal that this “plug-and-play” modification yields immediate performance gains. For instance, LSG- K^2 VAE achieves a significant reduction in CRPS on the *Weather* dataset, confirming that our proposed paradigm serves as a robust, model-agnostic plugin for boosting probabilistic forecasting performance.

4.5 Qualitative Analysis

We visualize the forecasting results on *ETTh1* ($L = 96, H = 96$) in Figure 4, comparing LSG-VAE against the K^2 VAE and advanced point forecasters equipped with prob-

abilistic heads (Koopa, PatchTST). As illustrated, LSG-VAE demonstrates superior adaptability, effectively capturing intrinsic volatility dynamics. Specifically, the confidence intervals (CIs) generated by LSG-VAE are sharp and dynamically responsive—they expand during volatile periods and contract in stable regimes. This stands in sharp contrast to the baselines, which suffer from severe uncertainty bloating: K^2 VAE, Koopa, and PatchTST produce excessively wide and nearly uniform intervals that fail to mimic the temporal rhythm of the data. This visual evidence confirms that merely grafting a Gaussian head onto deterministic backbones or using standard reconstruction losses leads to under-confident estimation, whereas LSG-VAE successfully captures the dynamic heteroscedasticity.

4.6 Efficiency Analysis

Beyond forecasting performance, computational efficiency is paramount for real-world deployment. We evaluate the inference latency (batch size=1) and memory usage on *ETTh2* using a single NVIDIA RTX 4090, with 100 samples generated for probabilistic baselines. As illustrated in Figure 5, LSG-VAE achieves the optimal trade-off between accuracy and speed. Unlike diffusion models that require hundreds of expensive iterative denoising steps, LSG-VAE generates the entire future horizon in a single non-autoregressive forward pass. This structural advantage results in orders-of-magnitude faster inference and a significantly lower memory footprint, rendering LSG-VAE highly suitable for time-critical streaming applications.

5 Conclusions

We presented LSG-VAE, a streamlined non-autoregressive framework designed to capture the dynamic heteroscedasticity inherent in real-world time series. Experiments confirm that, by replacing the rigid MSE objective with a Location-Scale likelihood, LSG-VAE establishes a new state-of-the-art balance between forecasting accuracy, uncertainty calibration, and computational efficiency. Moreover, the proven universality of the LSG mechanism suggests a promising direction for future probabilistic time series forecasting research: shifting focus from complex model design to theoretically grounded uncertainty quantification.

Impact Statement

This paper presents work whose goal is to advance the field of Machine Learning. There are many potential societal consequences of our work, none which we feel must be specifically highlighted here.

References

- Alexandrov, A., Benidis, K., Bohlke-Schneider, M., Flunkert, V., Gasthaus, J., Januschowski, T., Maddix, D. C., Rangapuram, S., Salinas, D., Schulz, J., Stella, L., Türkmen, A. C., and Wang, Y. GluonTS: Probabilistic and neural time series modeling in python. *J. Mach. Learn. Res.*, 21(116):1–6, 2020.
- Bengio, S., Vinyals, O., Jaitly, N., and Shazeer, N. Scheduled Sampling for Sequence Prediction with Recurrent Neural Networks. In *Advances in Neural Inf. Process. Syst.*, pp. 1171–1179, 2015.
- Cao, W., Wang, D., Li, J., Zhou, H., Li, L., and Li, Y. BRITS: Bidirectional Recurrent Imputation for Time Series. In *Advances in Neural Inf. Process. Syst.*, pp. 6776–6786, 2018.
- Desai, A., Freeman, C., Wang, Z., and Beaver, I. TimeVAE: A variational auto-encoder for multivariate time series generation. *arXiv preprint arXiv:2111.08095*, 2021.
- Gal, Y. and Ghahramani, Z. Dropout as a Bayesian Approximation: Representing Model Uncertainty in Deep Learning. In *Proc. Int. Conf. Mach. Learn.*, pp. 1050–1059, 2016.
- Gao, H., Shen, W., Qiu, X., Xu, R., Yang, B., and Hu, J. SSD-TS: Exploring the Potential of Linear State Space Models for Diffusion Models in Time Series Imputation. In *Proc. ACM SIGKDD Int. Conf. Knowledge discovery & data mining*, pp. 649–660, 2025.
- Gneiting, T. and Raftery, A. E. Strictly Proper Scoring Rules, Prediction, and Estimation. *J. Amer. Statist. Assoc.*, 102(477):359–378, 2007.
- Gneiting, T., Balabdaoui, F., and Raftery, A. E. Probabilistic forecasts, calibration and sharpness. *Journal of the Royal Statistical Society Series B: Statistical Methodology*, 69(2):243–268, 2007.
- Gu, A. and Dao, T. Mamba: Linear-time sequence modeling with selective state spaces. *arXiv preprint arXiv:2312.00752*, 2023.
- Hong, T. and Fan, S. Probabilistic electric load forecasting: A tutorial review. *Int. J. Forecasting*, 32(3):914–938, 2016.
- Huang, X., Yang, Y., Wang, Y., Wang, C., Zhang, Z., Xu, J., Chen, L., and Vazirgiannis, M. DGraph: A Large-Scale Financial Dataset for Graph Anomaly Detection. In *Advances in Neural Inf. Process. Syst.*, pp. 22765–22777, 2022.
- Kendall, A. and Gal, Y. What uncertainties do we need in bayesian deep learning for computer vision? In *Advances in Neural Inf. Process. Syst.*, pp. 5580–5590, 2017.
- Kim, T., Kim, J., Tae, Y., Park, C., Choi, J., and Jaegul, C. Reversible Instance Normalization for Accurate Time-Series Forecasting against Distribution Shift. In *Proc. Int. Conf. Learn. Representations*, pp. 1–25, 2022.
- Kingma, D. P. and Welling, M. Auto-Encoding Variational Bayes. In *Proc. Int. Conf. Learn. Representations*, pp. 1–14, 2014.
- Kolloviev, M., Ansari, A. F., Bohlke-Schneider, M., Zschiegner, J., Wang, H., and Wang, Y. B. Predict, Refine, Synthesize: Self-guiding diffusion models for probabilistic time series forecasting. In *Advances in Neural Inf. Process. Syst.*, pp. 28341–28364, 2023.
- Kong, X., Chen, Z., Liu, W., Ning, K., Zhang, L., Muhammad Marier, S., Liu, Y., Chen, Y., and Xia, F. Deep learning for time series forecasting: a survey. *International Journal of Machine Learning and Cybernetics*, pp. 1–34, 2025.
- Lázaro-Gredilla, M. and Titsias, M. K. Variational Heteroscedastic Gaussian Process Regression. In *Proc. Int. Conf. Mach. Learn.*, pp. 841–848, 2011.
- Li, Y., Yu, R., Shahabi, C., and Liu, Y. Diffusion Convolutional Recurrent Neural Network: Data-Driven Traffic Forecasting. In *Proc. Int. Conf. Learn. Representations*, pp. 1–16, 2018.
- Li, Y., Chen, W., Hu, X., Chen, B., Sun, B., and Zhou, M. Transformer-modulated diffusion models for probabilistic multivariate time series forecasting. In *Proc. Int. Conf. Learn. Representations*, pp. 1–19, 2024.
- Lim, B. and Zohren, S. Time-series forecasting with deep learning: a survey. *Philosophical Transactions of the Royal Society A: Mathematical, Physical and Engineering Sciences*, 379(2194):20200209, 2021.
- Liu, Q. and Paparrizos, J. The Elephant in the Room: Towards A Reliable Time-Series Anomaly Detection Benchmark. In *Advances in Neural Inf. Process. Syst.*, pp. 108231–108261, 2024.
- Liu, Y., Li, C., Wang, J., and Long, M. Koopa: Learning non-stationary time series dynamics with koopman predictors. In *Advances in Neural Inf. Process. Syst.*, pp. 12271–12290, 2023.

- Liu, Y., Hu, T., Zhang, H., Wu, H., Wang, S., Ma, L., and Long, M. iTransformer: Inverted Transformers Are Effective for Time Series Forecasting. In *Proc. Int. Conf. Learn. Representations*, pp. 1–25, 2024.
- Makansi, O., Ilg, E., Cicek, O., and Brox, T. Overcoming Limitations of Mixture Density Networks: A Sampling and Fitting Framework for Multimodal Future Prediction. In *Proc. IEEE Conf. Comp. Vis. Patt. Recogn.*, pp. 7144–7153, 2019.
- Miao, H., Xu, R., Zhao, Y., Wang, S., Wang, J., Yu, P. S., and Jensen, C. S. A parameter-efficient federated framework for streaming time series anomaly detection via lightweight adaptation. *IEEE Transactions on Mobile Computing*, 2025.
- Narayan Shukla, S. and Marlin, B. Heteroscedastic Temporal Variational Autoencoder For Irregularly Sampled Time Series . In *Proc. Int. Conf. Learn. Representations*, pp. 1–20, 2022.
- Nie, Y., Nguyen, N. H., Sinthong, P., and Kalagnanam, J. A Time Series is Worth 64 Words: Long-term Forecasting with Transformers. In *Proc. Int. Conf. Learn. Representations*, pp. 1–24, 2023.
- Paszke, A., Gross, S., Massa, F., Lerer, A., Bradbury, J., Chanan, G., Killeen, T., Lin, Z., Gimelshein, N., Antiga, L., Desmaison, A., Kopf, A., Yang, E., DeVito, Z., Raison, M., Tejani, A., Chilamkurthy, S., Steiner, B., Fang, L., Bai, J., and Chintala, S. PyTorch: An Imperative Style, High-Performance Deep Learning Library. In *Advances in Neural Inf. Process. Syst.*, pp. 8026–8037, 2019.
- Pessoa, P., Campitelli, P., Shepherd, D. P., Ozkan, S. B., and Pressé, S. Mamba time series forecasting with uncertainty quantification. *Machine Learning: Science and Technology*, 6:035012, 2025.
- Rangapuram, S. S., Seeger, M. W., Gasthaus, J., Stella, L., Wang, Y., and Januschowski, T. Deep state space models for time series forecasting. In *Advances in Neural Inf. Process. Syst.*, pp. 7796–7805, 2018.
- Rasul, K., Seward, C., Schuster, I., and Vollgraf, R. Autoregressive Denoising Diffusion Models for Multivariate Probabilistic Time Series Forecasting. In *Proc. Int. Conf. Mach. Learn.*, pp. 8857–8868, 2021a.
- Rasul, K., Sheikh, A., Schuster, I., Bergmann, U. M., and Vollgraf, R. Multivariate Probabilistic Time Series Forecasting via Conditioned Normalizing Flows. In *Proc. Int. Conf. Learn. Representations*, pp. 1–19, 2021b.
- Rigby, R. A. and Stasinopoulos, D. M. Generalized additive models for location, scale and shape. *Journal of the Royal Statistical Society Series C: Applied Statistics*, 54(3):507–554, 2005.
- Salinas, D., Flunkert, V., Gasthaus, J., and Januschowski, T. DeepAR: Probabilistic Forecasting with Autoregressive Recurrent Networks. *Int. J. Forecasting*, 36(3):1181–1191, 2020.
- Sezer, O. B., Gudelek, M. U., and Ozbayoglu, A. M. Financial time series forecasting with deep learning: A systematic literature review: 2005–2019. *Appl. Soft Comput.*, 90:106181, 2020.
- Shen, L. and Kwok, J. Non-autoregressive conditional diffusion models for time series prediction. In *Proc. Int. Conf. Mach. Learn.*, pp. 31016–31029, 2023.
- Sun, Y., Xie, Z., Wang, H., Huang, X., and Hu, Q. Solar wind speed prediction via graph attention network. *Space Weather*, 20(7), 2022.
- Tashiro, Y., Song, J., Song, Y., and Ermon, S. CSDI: Conditional Score-based Diffusion Models for Probabilistic Time Series Imputation. In *Advances in Neural Inf. Process. Syst.*, pp. 24804–24816, 2021.
- Wang, C., Zhuang, Z., Qi, Q., Wang, J., Wang, X., Sun, H., and Liao, J. Drift doesn’t matter: Dynamic decomposition with diffusion reconstruction for unstable multivariate time series anomaly detection. In *Advances in Neural Inf. Process. Syst.*, pp. 10758–10774, 2023.
- Wang, H., Wang, Z., Niu, Y., Liu, Z., Li, H., Liao, Y., Huang, Y., and Liu, X. An Accurate and Interpretable Framework for Trustworthy Process Monitoring. *IEEE Trans. Artif. Intell.*, 5(5):2241–2252, 2024a.
- Wang, H., li, z., Li, H., Chen, X., Gong, M., BinChen, and Chen, Z. Optimal Transport for Time Series Imputation. In *Proc. Int. Conf. Learn. Representations*, pp. 1–25, 2025.
- Wang, J., Du, W., Yang, Y., Qian, L., Cao, W., Zhang, K., Wang, W., Liang, Y., and Wen, Q. Deep learning for multivariate time series imputation: A survey. *arXiv preprint arXiv:2402.04059*, 2024b.
- Wu, X., Qiu, X., Gao, H., Hu, J., Yang, B., and Guo, C. K²VAE: A Koopman-Kalman Enhanced Variational AutoEncoder for Probabilistic Time Series Forecasting. In *Proc. Int. Conf. Mach. Learn.*, pp. 1–22, 2025a.
- Wu, X., Qiu, X., Li, Z., Wang, Y., Hu, J., Guo, C., Xiong, H., and Yang, B. CATCH: Channel-Aware multivariate Time Series Anomaly Detection via Frequency Patching. In *Proc. Int. Conf. Learn. Representations*, pp. 56894–56922, 2025b.
- Xu, J., Wu, H., Wang, J., and Long, M. Anomaly Transformer: Time Series Anomaly Detection with Association Discrepancy. In *Proc. Int. Conf. Learn. Representations*, pp. 1–20, 2022.

Xu, Y., Zeng, A., and Xu, Q. FITS: Modeling Time Series with 10k Parameters. In *Proc. Int. Conf. Learn. Representations*, pp. 1–24, 2024.

Ye, W., Xu, Z., and Gui, N. Non-stationary Diffusion for Probabilistic Time Series Forecasting. In *Proc. Int. Conf. Mach. Learn.*, pp. 1–19, 2025.

Yuan, X. and Qiao, Y. Diffusion-TS: Interpretable Diffusion for General Time Series Generation. In *Proc. Int. Conf. Learn. Representations*, pp. 1–29, 2024.

Zhang, J., Wen, X., Zhang, Z., Zheng, S., Li, J., and Bian, J. ProbTS: Benchmarking Point and Distributional Forecasting across Diverse Prediction Horizons. In *Advances in Neural Inf. Process. Syst.*, pp. 48045–48082, 2024.

A Related Works

A.1 Heteroscedasticity and Distributional Forecasting

Quantifying the stochastic uncertainty inherent in future states—specifically the time-varying volatility (heteroscedasticity)—has long been a central pursuit in probabilistic forecasting. Research in this domain can be broadly categorized into deep autoregressive models, distributional regression, and stochastic process-based approaches.

Deep Autoregressive Paradigms Seminal works like DeepAR (Salinas et al., 2020) pioneered the use of Recurrent Neural Networks (RNNs) to model hidden state transitions, estimating likelihood parameters at each time step. While initially formulated with Gaussian likelihoods, subsequent extensions in libraries like GluonTS (Alexandrov et al., 2020) have incorporated heavy-tailed distributions to enhance robustness. Similarly, DeepState (Rangapuram et al., 2018) hybridizes state space models with RNNs. However, despite their distributional flexibility, these methods rely on recursive decoding, which precludes parallelization and inherently suffers from error accumulation over long forecasting horizons.

Distributional Regression and MDNs Beyond simple parametric shapes, advanced distributional regression techniques have been adapted for forecasting. GAMLSS (Rigby & Stasinopoulos, 2005) provides a rigorous statistical framework for modeling location, scale, and shape parameters. To capture multimodal densities, Mixture Density Networks (MDNs) (Makansi et al., 2019) output a weighted combination of distributions. While powerful, MDNs are notoriously difficult to train due to numerical instabilities and mode collapse, and they are typically applied in step-wise regression settings rather than global sequence generation.

Gaussian Processes and Volatility Models Bayesian non-parametric methods offer principled uncertainty quantification. Heteroscedastic Gaussian Processes (Lázaro-Gredilla & Titsias, 2011) explicitly model input-dependent volatility. However, GP-based methods generally suffer from cubic computational complexity $\mathcal{O}(N^3)$, limiting their scalability to long multivariate time series. Similarly, traditional volatility models often focus on financial return modeling rather than general-purpose long-term forecasting.

A.2 Generative Forecasting Paradigms

To overcome the expressiveness limitations of parametric models, deep generative models have surged in prominence. We review three mainstream categories: iterative diffusion models, emerging state space models, and variational latent variable models.

Iterative Denoising Models Denoising Diffusion Probabilistic Models (DDPMs), such as TimeGrad (Rasul et al., 2021a) and CSDI (Tashiro et al., 2021), formulate forecasting as a conditional denoising process. Recent advancements like NsDiff (Ye et al., 2025) and DiffusionTS (Yuan & Qiao, 2024) further adapt this framework to handle non-stationary characteristics. While diffusion models offer superior distributional expressiveness, they face a severe efficiency bottleneck: the requirement for dozens or hundreds of iterative denoising steps renders them computationally expensive for real-time applications.

State Space Models (SSMs) Recently, Structured State Space Models like Mamba (Gu & Dao, 2023) have emerged, offering linear scaling complexity $\mathcal{O}(L)$. Approaches such as Mamba-ProbTSF (Pessoa et al., 2025) attempt to adapt this architecture for probabilistic tasks. While highly efficient for long sequences, these models typically function as generic sequence encoders. Unlike dedicated generative frameworks, they often lack explicit mechanisms to structurally decouple signal from noise, potentially leading to over-smoothed uncertainty estimates when confronting rapid regime changes or extreme volatility.

Variational Autoencoders (VAEs) and Heteroscedasticity VAEs offer a compelling balance between capability and efficiency via one-step generation. Standard forecasting approaches, such as TimeVAE (Desai et al., 2021) and the state-of-the-art K^2 VAE (Wu et al., 2025a), excel in modeling long-term nonlinearity but predominantly rely on MSE-based reconstruction, implicitly assuming a fixed-variance Gaussian likelihood. While models like HeTVAE (Narayan Shukla & Marlin, 2022) have successfully integrated heteroscedastic modeling into the VAE framework, they are primarily tailored for imputation and irregularly sampled data, often necessitating complex attention mechanisms or ODE solvers that differ significantly from the requirements of efficient long-term forecasting. Thus, a gap remains for a forecasting-specialized framework that is both computationally lightweight (like K^2 VAE) and probabilistically rigorous in capturing dynamic volatility.

Bridging the Gap via Unified Modeling Our proposed LSG-VAE transcends this dichotomy. Rather than merely grafting heteroscedastic objectives onto a complex backbone, we propose a paradigm shift towards Non-autoregressive Heteroscedastic Modeling. We challenge the prevailing assumption that dynamic volatility requires recursive decoding (as in DeepAR) or expensive iterative sampling (as in Diffusion). By theoretically aligning the Location-Scale likelihood with global latent dynamics, LSG-VAE synthesizes the distributional rigor of statistical approaches with the parallel efficiency of deep generative models. This results in a streamlined framework that naturally disentangles the underlying trend from aleatoric uncertainty without incurring the computational penalties of prior art. Consistent with this positioning, our experimental evaluation primarily benchmarks against leading state-of-the-art generative models (e.g., Diffusion, VAEs) and advanced point forecasters (e.g., Transformers), omitting earlier autoregressive or statistical baselines that have been consistently outperformed in recent literature.

B Theoretical Analysis

In this section, we provide the theoretical derivations supporting the LSG-VAE framework. We strictly derive the heteroscedastic objective from the variational lower bound, analyze the gradient dynamics to prove the adaptive attenuation mechanism, and demonstrate the model’s theoretical robustness to outliers compared to standard MSE-based approaches.

B.1 Derivation of the Heteroscedastic ELBO

The standard Variational Autoencoder (VAE) maximizes the Evidence Lower Bound (ELBO) of the marginal likelihood $p_\theta(\mathcal{X})$. For a time series \mathcal{X} and latent variable \mathbf{Z} , the ELBO is defined as:

$$\mathcal{L}_{\text{ELBO}} = \mathbb{E}_{q_\phi(\mathbf{Z}|\mathcal{X})}[\log p_\theta(\mathcal{X}|\mathbf{Z})] - D_{KL}(q_\phi(\mathbf{Z}|\mathcal{X}) \parallel p(\mathbf{Z})). \quad (11)$$

We focus on the reconstruction term $\mathcal{L}_{rec} = \mathbb{E}_{q_\phi}[\log p_\theta(\mathcal{X}|\mathbf{Z})]$.

In vanilla VAEs, the decoder assumes a fixed variance $\sigma^2 = c$, implying $p_\theta(\mathbf{x}_t|\mathbf{Z}) = \mathcal{N}(\boldsymbol{\mu}_t, c\mathbf{I})$. This simplifies to the standard MSE loss:

$$\log p_\theta(\mathcal{X}|\mathbf{Z}) \propto - \sum_t \|\mathbf{x}_t - \boldsymbol{\mu}_t\|_2^2 + \text{const}. \quad (12)$$

In LSG-VAE, we relax this assumption to model a heteroscedastic Gaussian Likelihood, where both mean $\boldsymbol{\mu}_t$ and variance σ_t^2 are functions of \mathbf{Z} :

$$p_\theta(\mathbf{x}_t|\mathbf{Z}) = \prod_{c=1}^C \frac{1}{\sqrt{2\pi}\sigma_{t,c}} \exp\left(-\frac{(\mathbf{x}_{t,c} - \boldsymbol{\mu}_{t,c})^2}{2\sigma_{t,c}^2}\right). \quad (13)$$

Taking the log-likelihood:

$$\begin{aligned} \log p_\theta(\mathbf{x}_t|\mathbf{Z}) &= \sum_{c=1}^C \left[-\log(\sqrt{2\pi}) - \log(\sigma_{t,c}) - \frac{(\mathbf{x}_{t,c} - \boldsymbol{\mu}_{t,c})^2}{2\sigma_{t,c}^2} \right] \\ &\propto - \sum_{c=1}^C \left(\log \sigma_{t,c} + \frac{(\mathbf{x}_{t,c} - \boldsymbol{\mu}_{t,c})^2}{2\sigma_{t,c}^2} \right). \end{aligned} \quad (14)$$

Maximizing this term is equivalent to minimizing the Negative Log-Likelihood (NLL) defined in Eq. (9) in the main text. This confirms that our Location-Scale loss is strictly derived from the variational inference framework under a heteroscedastic assumption.

B.2 Proof of Adaptive Attenuation Mechanism

We formally prove how the learned scale parameter σ acts as an adaptive weight to modulate the learning of the location parameter μ .

Consider the loss function for a single data point x (omitting subscripts for brevity):

$$J(\mu, \sigma) = \frac{1}{2} \log \sigma^2 + \frac{(x - \mu)^2}{2\sigma^2}. \quad (15)$$

We analyze the gradient descent dynamics with respect to the network parameters. Let θ be the parameters of the decoder such that $\mu = f_\theta(z)$ and $\sigma = g_\theta(z)$. By the chain rule, the update to θ via the location head is proportional to $\frac{\partial J}{\partial \mu}$:

$$\frac{\partial J}{\partial \mu} = \frac{\partial}{\partial \mu} \left(\frac{(x - \mu)^2}{2\sigma^2} \right) = -\frac{1}{\sigma^2}(x - \mu). \quad (16)$$

Proposition 1 (Gradient Scaling). *The gradient magnitude for the location parameter is inversely proportional to the predicted variance σ^2 .*

Proof. From the equation above, the effective learning rate for the reconstruction error $(x - \mu)$ is scaled by the factor $\lambda = \frac{1}{\sigma^2}$. This results in a dynamic adjustment mechanism: in the Low Uncertainty Regime ($\sigma \rightarrow 0$), where the model is confident, $\lambda \rightarrow \infty$, causing the model to aggressively minimize the residual $(x - \mu)$ akin to strict L_2 regression. Conversely, in the High Uncertainty Regime ($\sigma \rightarrow \infty$), which typically corresponds to noisy data or outliers, $\lambda \rightarrow 0$. Consequently, the gradient vanishes, effectively “ignoring” such data points during the update of μ . This mechanism, which we term *Adaptive Attenuation*, prevents transient stochastic fluctuations or outliers from corrupting the trend estimation (Location Head).

B.3 Robustness Analysis: Comparison with MSE

Here we demonstrate that LSG-VAE is theoretically more robust to outliers than standard VAEs (MSE).

Scenario. Consider a scenario where the ground truth is subject to a large volatility spike or outlier, such that the residual $r = |x - \mu|$ is very large ($r \rightarrow \infty$).

Case 1: Fixed Variance (MSE). For a standard VAE with fixed $\sigma = 1$:

$$\mathcal{L}_{MSE} \propto (x - \mu)^2. \quad (17)$$

The loss grows quadratically. The influence of the outlier on the gradient is linear with respect to the error magnitude, causing the mean μ to shift significantly towards the outlier.

Case 2: Learned Variance (LSG-VAE). The model simultaneously optimizes σ . Taking the partial derivative of $J(\mu, \sigma)$ w.r.t σ and setting to 0 to find the optimal σ^* for a given fixed residual r :

$$\frac{\partial J}{\partial \sigma} = \frac{1}{\sigma} - \frac{r^2}{\sigma^3} = 0 \implies \sigma^* = |x - \mu|. \quad (18)$$

This implies that for an outlier, the optimal strategy for the model is to increase uncertainty σ to match the residual. Substituting $\sigma^* = |x - \mu|$ back into the loss function J :

$$\begin{aligned} J(\mu, \sigma^*) &= \log |x - \mu| + \frac{(x - \mu)^2}{2(x - \mu)^2} \\ &= \log |x - \mu| + \frac{1}{2}. \end{aligned} \quad (19)$$

In conclusion, in the presence of outliers, the effective loss function of LSG-VAE transitions from quadratic (L_2) to logarithmic. Since $\lim_{r \rightarrow \infty} \log(r) \ll r^2$, the penalty assigned to outliers by LSG-VAE is orders of magnitude smaller than that of MSE. This proves that LSG-VAE possesses inherent robust regression properties similar to the Lorentzian loss, automatically mitigating the impact of non-stationary volatility.

C Experimental Details

C.1 Datasets

To ensure a rigorous and comprehensive evaluation, we conduct experiments on widely-recognized real-world benchmarks spanning diverse domains including Energy, Transportation, Weather, Economics, and Health. Consistent with the experimental design in Section 4, our evaluation is divided into two distinct settings:

Setting I: Comprehensive Benchmarking (ProbTS Protocol). Following the standard long-term forecasting protocol used in ProbTS (Zhang et al., 2024) and K^2 VAE (Wu et al., 2025a), we utilize nine multivariate datasets: *ETTh1*, *ETTh2*, *ETTm1*,

ETTh2, *Electricity*, *Traffic*, *Weather*, *Exchange*, and *ILI*. The look-back window is fixed at $L = 96$ for all datasets except *ILI*, where $L = 36$. The forecasting horizon H is evaluated at $\{96, 192, 336, 720\}$ steps (for *ILI*, $H \in \{24, 36, 48, 60\}$).

Setting II: Generative Benchmarking (NsDiff Protocol). To evaluate the generative quality and calibration against diffusion baselines, we follow the specific protocol adopted by NsDiff (Ye et al., 2025). We use 8 datasets: *ETTh1*, *ETTh2*, *ETTh1*, *ETTh2*, *Electricity*, *Traffic*, *Exchange*, and *ILI*. In this setting, the input length is fixed at $L = 168$ (except *ILI*), which is the standard configuration for validating distributional properties in recent diffusion literature.

Table 5 provides detailed statistics for all datasets used in our experiments.

Table 5. Statistics of the multivariate time series datasets.

Dataset	Features (C)	Timesteps	Frequency	Domain
ETTh1	7	17,420	1 Hour	Energy
ETTh2	7	17,420	1 Hour	Energy
ETTh1	7	69,680	15 Min	Energy
ETTh2	7	69,680	15 Min	Energy
Electricity	321	26,304	1 Hour	Energy
Traffic	862	17,544	1 Hour	Transport
Weather	21	52,696	10 Min	Weather
Exchange	8	7,588	1 Day	Economics
ILI	7	966	1 Week	Health

C.2 Baselines

We compare LSG-VAE against a comprehensive set of 15 competitive baselines, categorized into two groups based on their modeling paradigms.

The first group consists of Deep Point Forecasters equipped with probabilistic heads. Since standard point forecasters do not naturally output distributions, we augment them with a Gaussian head to predict mean and variance, trained via NLL loss. This category includes FITS (Xu et al., 2024), a frequency-domain interpolation based model; PatchTST (Nie et al., 2023), a state-of-the-art transformer utilizing patching and channel-independence; iTransformer (Liu et al., 2024), which embeds the entire time series as a token; and Koopa (Liu et al., 2023), a dynamics-aware model based on Koopman operator theory.

The second group comprises Generative and Probabilistic Models, covering VAE, flow, and diffusion-based architectures. Specifically, we compare against the VAE-based K^2 VAE (Wu et al., 2025a), the previous SOTA method that disentangles key and key-response series. For flow-based methods, we include TimeGrad (Rasul et al., 2021a), an autoregressive model using normalizing flows; GRU NVP and GRU MAF, which combine RNNs with flow-based density estimation; and Trans-MAF (Rasul et al., 2021b), a transformer-based flow model. Regarding diffusion-based approaches, we select CSDI (Tashiro et al., 2021), a conditional score-based diffusion model; TimeDiff (Shen & Kwok, 2023), which introduces future mixup; DiffusionTS (Yuan & Qiao, 2024), using transformer-based diffusion; TMDM (Li et al., 2024), exploring metric-tailored diffusion; NsDiff (Ye et al., 2025), a non-stationary diffusion model; and TSDiff (Kollovich et al., 2023), a soft-diffusion approach.

C.3 Evaluation Metrics

We adopt three complementary metrics to evaluate forecasting performance:

Continuous Ranked Probability Score (CRPS). CRPS measures the compatibility between the predicted distribution and the observation. It is a strictly proper scoring rule defined as:

$$\text{CRPS}(F, x) = \int_{\mathbb{R}} (F(z) - \mathbb{I}\{x \leq z\})^2 dz, \quad (20)$$

where F is the predictive Cumulative Distribution Function (CDF) and x is the ground truth. We approximate CRPS using 100 Monte Carlo samples.

Normalized Mean Absolute Error (NMAE). NMAE assesses the accuracy of the point forecast (median or mean of the samples). It is scale-invariant, facilitating comparison across datasets:

$$\text{NMAE} = \frac{\sum_{t,k} |x_{t,k} - \hat{x}_{t,k}|}{\sum_{t,k} |x_{t,k}|}. \quad (21)$$

Quantile Interval Calibration Error (QICE). QICE strictly evaluates the reliability of the confidence intervals. It measures the mean absolute deviation between the empirical coverage $\hat{c}(q)$ and the nominal quantile level q :

$$\text{QICE} = \frac{1}{M} \sum_{m=1}^M |\hat{c}(q_m) - q_m|, \quad (22)$$

where we use quantile levels $q \in \{0.1, 0.2, \dots, 0.9\}$. Lower QICE indicates better calibration.

C.4 Implementation Details

Model Architecture The LSG-VAE is built upon a standard encoder-decoder architecture. To ensure a fair comparison with the primary baseline K^2 VAE (Wu et al., 2025a), we adopt the same patching strategy (patch length $P = 24$) and a lightweight MLP-based encoder. The core innovation lies in the Location-Scale Decoder. Unlike standard VAEs that typically output a single reconstruction vector, our decoder features a dual-head structure to explicitly model heteroscedasticity. Specifically, the decoder bifurcates into two parallel branches: a Location Head, which utilizes a linear projection layer to output the location parameter μ_t , and a Scale Head, which employs a linear layer followed by a `Softplus` activation to output the scale parameter σ_t . This design allows the model to maximize the heteroscedastic Gaussian Likelihood \mathcal{L}_{NLL} as detailed in Eq. (9).

Training Protocol We implement LSG-VAE using PyTorch (Paszke et al., 2019). All experiments are conducted on a single NVIDIA GeForce RTX 4090 GPU (24GB). The model is optimized using the Adam optimizer with an initial learning rate of 10^{-3} (dataset-specific adjustments are made within the range $[10^{-4}, 10^{-3}]$). We use a batch size of 32 by default. The training objective is the ELBO, comprising the Location-Scale NLL loss (reconstruction & prediction) and the KL divergence term. We train the model for a maximum of 50 epochs with an early stopping strategy (patience=10). To facilitate reproducibility, the source code and configuration files are available at <https://anonymous.4open.science/r/LSG-VAE>.

C.5 Full Results

We present the complete benchmarking results for Long-term Probabilistic Time Series Forecasting (LPTSF) in Table 6 and Table 7, covering all four forecasting horizons ($H \in \{96, 192, 336, 720\}$) across nine real-world datasets. The comprehensive evaluation reveals that LSG-VAE achieves a dominant performance lead. Crucially, it not only surpasses specialized generative models (e.g., Diffusion and Flow-based methods) in terms of distributional fidelity (CRPS) but also consistently outperforms state-of-the-art point forecasters on deterministic metrics (NMAE). This confirms that the proposed Location-Scale paradigm effectively captures long-term dependencies and complex volatility dynamics.

Furthermore, we provide a detailed efficiency analysis to validate the model’s suitability for real-world deployment. As evidenced by the comparison, LSG-VAE exhibits superior computational efficiency, characterized by low memory overhead and rapid inference speeds. In sharp contrast to iterative diffusion models or autoregressive baselines, LSG-VAE achieves high-precision forecasting with orders-of-magnitude lower latency, striking an optimal balance between accuracy and efficiency.

Embracing Heteroscedasticity for Probabilistic Time Series Forecasting

Table 6. Results of CRPS (mean_{std}) on long-term forecasting scenarios, each containing five independent runs with different seeds. The context length is set to 36 for the ILI dataset and 96 for the others. Lower CRPS values indicate better predictions. The means and standard errors are based on 5 independent runs of retraining and evaluation. **Red**: the best, **Blue**: the 2nd best.

Dataset	Horizon	Koopa	iTransformer	FITS	PatchTST	GRU MAF	Trans MAF	TSDiff	CSDI	TimeGrad	GRU NVP	K ² VAE	LSG-VAE
ETTm1	96	0.285±0.018	0.301±0.033	0.267±0.023	0.261±0.051	0.295±0.055	0.313±0.045	0.344±0.050	0.236±0.006	0.522±0.105	0.383±0.053	<u>0.232±0.010</u>	0.208±0.009
	192	0.289±0.024	0.314±0.023	0.261±0.022	0.275±0.030	0.389±0.033	0.424±0.029	0.345±0.035	0.291±0.025	0.603±0.092	0.396±0.030	<u>0.259±0.013</u>	0.240±0.010
	336	0.286±0.035	0.311±0.029	0.275±0.030	0.285±0.028	0.429±0.021	0.481±0.019	0.462±0.043	0.322±0.033	0.601±0.028	0.486±0.032	<u>0.262±0.030</u>	0.251±0.022
	720	0.295±0.027	0.455±0.021	0.305±0.024	0.304±0.029	0.536±0.033	0.688±0.043	0.478±0.027	0.448±0.038	0.621±0.037	0.546±0.036	<u>0.294±0.026</u>	0.279±0.020
ETTm2	96	0.178±0.023	0.181±0.031	0.162±0.053	0.142±0.034	0.177±0.024	0.227±0.013	0.175±0.019	<u>0.115±0.009</u>	0.427±0.042	0.319±0.044	0.126±0.007	0.107±0.005
	192	0.185±0.014	0.190±0.010	0.185±0.053	0.172±0.023	0.411±0.026	0.253±0.037	0.255±0.029	<u>0.147±0.008</u>	0.424±0.061	0.326±0.025	0.148±0.009	0.129±0.007
	336	0.198±0.015	0.206±0.055	0.218±0.053	0.195±0.042	0.377±0.023	0.253±0.013	0.328±0.047	0.190±0.018	0.469±0.049	0.449±0.145	<u>0.164±0.010</u>	0.147±0.010
	720	0.233±0.025	0.311±0.024	0.449±0.034	0.229±0.036	0.272±0.029	0.355±0.043	0.344±0.046	0.239±0.035	0.470±0.054	0.561±0.273	<u>0.221±0.023</u>	0.166±0.018
ETTh1	96	0.307±0.033	0.292±0.032	0.294±0.023	0.312±0.036	0.293±0.037	0.333±0.045	0.395±0.052	0.437±0.018	0.455±0.046	0.379±0.030	<u>0.264±0.020</u>	0.252±0.010
	192	0.301±0.014	0.298±0.020	0.304±0.028	0.313±0.034	0.348±0.075	0.351±0.063	0.467±0.044	0.496±0.051	0.516±0.038	0.425±0.019	<u>0.290±0.016</u>	0.277±0.012
	336	0.312±0.019	0.327±0.043	0.318±0.023	0.319±0.035	0.377±0.026	0.371±0.031	0.450±0.027	0.454±0.025	0.512±0.026	0.458±0.054	<u>0.308±0.021</u>	0.300±0.015
	720	0.318±0.009	0.350±0.019	0.348±0.025	0.323±0.020	0.393±0.043	0.363±0.053	0.516±0.027	0.528±0.012	0.523±0.027	0.502±0.039	<u>0.314±0.011</u>	0.310±0.012
ETTh2	96	0.199±0.012	0.185±0.013	0.187±0.011	0.197±0.021	0.239±0.019	0.263±0.020	0.336±0.021	0.164±0.013	0.358±0.026	0.432±0.141	<u>0.162±0.009</u>	0.148±0.005
	192	0.198±0.022	0.199±0.019	0.195±0.022	0.204±0.055	0.313±0.034	0.273±0.024	0.265±0.043	0.226±0.018	0.457±0.081	0.625±0.170	<u>0.186±0.018</u>	0.162±0.010
	336	0.262±0.019	0.271±0.033	0.246±0.044	0.277±0.054	0.376±0.034	0.265±0.042	0.350±0.031	0.274±0.022	0.481±0.078	0.793±0.319	<u>0.257±0.023</u>	0.175±0.016
	720	0.293±0.026	0.542±0.015	0.314±0.022	0.304±0.018	0.990±0.023	0.327±0.033	0.406±0.056	0.302±0.040	0.445±0.016	0.539±0.090	<u>0.280±0.014</u>	0.174±0.010
Electricity	96	0.110±0.004	0.102±0.004	0.105±0.006	0.126±0.005	0.083±0.009	0.088±0.014	0.344±0.006	0.153±0.137	0.096±0.002	0.094±0.003	<u>0.073±0.002</u>	0.069±0.002
	192	0.109±0.011	0.104±0.014	0.112±0.104	0.123±0.032	0.093±0.024	0.097±0.009	0.345±0.006	0.200±0.094	0.100±0.004	0.097±0.002	<u>0.080±0.004</u>	0.075±0.005
	336	0.121±0.011	0.104±0.010	0.111±0.014	0.131±0.024	0.095±0.001	-	0.462±0.054	-	0.102±0.007	0.099±0.001	<u>0.084±0.001*</u>	0.078±0.001
	720	0.113±0.018	0.109±0.044	0.115±0.024	0.127±0.015	0.106±0.007	-	0.478±0.005	-	0.108±0.003	0.114±0.013	<u>0.087±0.005*</u>	0.080±0.006
Traffic	96	0.297±0.019	0.256±0.004	0.258±0.004	0.194±0.002	0.215±0.003	0.208±0.004	0.294±0.003	-	0.202±0.004	0.187±0.002	<u>0.186±0.001*</u>	0.180±0.005
	192	0.308±0.009	0.250±0.002	0.275±0.003	0.198±0.004	-	-	0.306±0.004	-	0.208±0.003	0.192±0.001	<u>0.188±0.002*</u>	0.187±0.004
	336	0.334±0.017	0.261±0.001	0.327±0.001	0.204±0.002	-	-	0.317±0.006	-	0.213±0.003	0.201±0.004	<u>0.195±0.003</u>	0.194±0.002
	720	0.358±0.022	0.284±0.004	0.374±0.004	0.214±0.001	-	-	0.391±0.002	-	0.220±0.002	0.211±0.004	<u>0.190±0.001</u>	0.192±0.003
Weather	96	0.132±0.008	0.131±0.011	0.210±0.013	0.131±0.007	0.139±0.008	0.105±0.011	0.104±0.020	0.068±0.008	0.130±0.017	0.116±0.013	<u>0.080±0.007</u>	0.070±0.005
	192	0.133±0.017	0.132±0.018	0.205±0.019	0.131±0.014	0.143±0.020	0.142±0.022	0.134±0.012	0.068±0.006	0.127±0.019	0.122±0.021	<u>0.079±0.009</u>	0.067±0.006
	336	0.136±0.021	0.132±0.010	0.221±0.005	0.137±0.008	0.129±0.012	0.133±0.014	0.137±0.010	0.083±0.002	0.130±0.006	0.128±0.011	<u>0.082±0.010</u>	0.071±0.008
	720	0.140±0.007	0.133±0.004	0.267±0.003	0.142±0.005	0.122±0.006	0.113±0.004	0.152±0.003	0.087±0.003	0.113±0.011	0.110±0.004	<u>0.084±0.003</u>	0.073±0.003
Exchange	96	0.063±0.006	0.061±0.003	0.048±0.004	0.063±0.006	0.026±0.010	0.028±0.002	0.079±0.007	0.028±0.003	0.068±0.003	0.071±0.006	<u>0.031±0.002</u>	0.022±0.003
	192	0.065±0.020	0.062±0.010	0.049±0.011	0.067±0.008	0.034±0.009	0.046±0.017	0.093±0.011	0.045±0.003	0.087±0.013	0.068±0.004	<u>0.032±0.010</u>	0.030±0.008
	336	0.072±0.008	0.067±0.008	0.052±0.013	0.071±0.017	0.058±0.023	0.045±0.010	0.081±0.007	0.060±0.004	0.074±0.009	0.072±0.002	<u>0.048±0.004</u>	0.041±0.005
	720	0.091±0.012	0.087±0.023	0.074±0.011	0.097±0.007	0.160±0.019	0.148±0.017	0.082±0.010	0.143±0.020	0.099±0.015	0.079±0.009	<u>0.069±0.005</u>	0.065±0.004
ILI	24	0.245±0.018	0.212±0.013	0.233±0.015	0.312±0.014	0.097±0.010	0.092±0.019	0.228±0.024	0.250±0.013	0.275±0.047	0.257±0.003	<u>0.087±0.003</u>	0.082±0.003
	36	0.214±0.008	0.182±0.016	0.217±0.023	0.241±0.021	0.117±0.017	0.115±0.011	0.235±0.010	0.285±0.010	0.272±0.057	0.281±0.004	<u>0.113±0.005</u>	0.110±0.003
	48	0.271±0.021	0.213±0.012	0.185±0.026	0.242±0.018	0.128±0.019	0.133±0.022	0.265±0.039	0.285±0.036	0.295±0.033	0.288±0.008	<u>0.124±0.010</u>	0.114±0.008
	60	0.228±0.022	0.222±0.020	0.211±0.011	0.233±0.019	0.172±0.034	0.155±0.018	0.263±0.022	0.283±0.012	0.295±0.083	0.307±0.005	<u>0.142±0.008</u>	0.130±0.005

* denotes results that were reproduced by us due to obvious typographical errors in the originally reported values.

Embracing Heteroscedasticity for Probabilistic Time Series Forecasting

Table 7. Results of NMAE (mean_{std}) on long-term forecasting scenarios, each containing five independent runs with different seeds. The context length is set to 36 for the ILI dataset and 96 for the others. Lower NMAE values indicate better predictions. The means and standard errors are based on 5 independent runs of retraining and evaluation. **Red**: the best, **Blue**: the 2nd best.

Dataset	Horizon	Koopa	iTransformer	FITS	PatchTST	GRU MAF	Trans MAF	TSDiff	CSDI	TimeGrad	GRU NVP	K ² VAE	LSG-VAE
ETTm1	96	0.362±0.022	0.369±0.029	0.349±0.032	0.329±0.100	0.402±0.087	0.456±0.042	0.441±0.021	0.308±0.005	0.645±0.129	0.488±0.058	0.284±0.011	0.268±0.009
	192	0.365±0.032	0.384±0.041	0.341±0.032	0.338±0.022	0.476±0.046	0.553±0.012	0.441±0.019	0.377±0.026	0.748±0.084	0.514±0.042	0.323±0.020	0.309±0.012
	336	0.364±0.026	0.380±0.020	0.356±0.022	0.344±0.013	0.522±0.019	0.590±0.047	0.571±0.033	0.419±0.042	0.759±0.015	0.630±0.029	0.330±0.014	0.327±0.010
	720	0.377±0.037	0.490±0.038	0.406±0.072	0.382±0.066	0.711±0.081	0.822±0.034	0.622±0.045	0.578±0.051	0.793±0.034	0.707±0.050	0.373±0.032	0.367±0.023
ETTm2	96	0.225±0.039	0.221±0.039	0.210±0.040	0.216±0.035	0.212±0.082	0.279±0.031	0.224±0.033	0.146±0.012	0.525±0.047	0.413±0.059	0.144±0.011	0.134±0.010
	192	0.233±0.026	0.229±0.031	0.234±0.038	0.215±0.022	0.535±0.029	0.292±0.041	0.316±0.040	0.189±0.012	0.530±0.060	0.427±0.033	0.170±0.009	0.160±0.010
	336	0.267±0.023	0.245±0.049	0.276±0.019	0.234±0.024	0.407±0.043	0.309±0.032	0.397±0.051	0.248±0.024	0.566±0.047	0.580±0.169	0.187±0.021	0.158±0.015
	720	0.290±0.033	0.385±0.042	0.540±0.052	0.288±0.034	0.355±0.048	0.475±0.029	0.416±0.065	0.306±0.040	0.561±0.044	0.749±0.385	0.275±0.035	0.207±0.026
ETTh1	96	0.407±0.052	0.386±0.092	0.393±0.142	0.407±0.022	0.371±0.034	0.423±0.047	0.510±0.029	0.557±0.022	0.585±0.058	0.481±0.037	0.336±0.041	0.328±0.019
	192	0.396±0.022	0.388±0.041	0.406±0.079	0.405±0.088	0.430±0.022	0.451±0.012	0.596±0.056	0.625±0.065	0.680±0.058	0.531±0.018	0.372±0.023	0.365±0.015
	336	0.406±0.028	0.415±0.022	0.410±0.063	0.412±0.024	0.462±0.049	0.481±0.041	0.581±0.035	0.574±0.026	0.666±0.047	0.580±0.064	0.394±0.022	0.384±0.018
	720	0.412±0.008	0.449±0.022	0.468±0.012	0.428±0.024	0.496±0.019	0.455±0.025	0.657±0.017	0.657±0.014	0.672±0.015	0.643±0.046	0.396±0.012	0.389±0.013
ETTh2	96	0.249±0.015	0.234±0.011	0.243±0.009	0.247±0.028	0.292±0.012	0.345±0.042	0.421±0.033	0.214±0.018	0.448±0.031	0.548±0.158	0.189±0.010	0.183±0.009
	192	0.249±0.032	0.247±0.040	0.252±0.022	0.265±0.091	0.376±0.112	0.343±0.044	0.339±0.033	0.294±0.027	0.575±0.089	0.766±0.223	0.213±0.021	0.201±0.015
	336	0.274±0.027	0.297±0.029	0.291±0.032	0.314±0.045	0.454±0.057	0.333±0.078	0.427±0.041	0.353±0.028	0.606±0.095	0.942±0.408	0.263±0.039	0.221±0.020
	720	0.286±0.042	0.667±0.012	0.401±0.022	0.371±0.021	1.092±0.019	0.412±0.020	0.482±0.022	0.382±0.030	0.550±0.018	0.688±0.161	0.278±0.020	0.223±0.015
Electricity	96	0.146±0.015	0.134±0.002	0.137±0.002	0.168±0.012	0.108±0.009	0.114±0.010	0.441±0.013	0.203±0.189	0.119±0.003	0.118±0.003	0.093±0.002	0.089±0.003
	192	0.143±0.023	0.137±0.022	0.143±0.112	0.163±0.032	0.120±0.033	0.131±0.008	0.441±0.005	0.264±0.129	0.124±0.005	0.121±0.003	0.102±0.010	0.096±0.008
	336	0.151±0.017	0.136±0.002	0.139±0.002	0.168±0.010	0.122±0.018	-	0.571±0.022	-	0.126±0.008	0.123±0.001	0.107±0.002	0.102±0.003
	720	0.149±0.025	0.140±0.009	0.149±0.012	0.164±0.024	0.136±0.098	-	0.622±0.142	-	0.134±0.004	0.144±0.017	0.117±0.019	0.111±0.012
Traffic	96	0.377±0.024	0.332±0.008	0.332±0.007	0.228±0.010	0.274±0.012	0.265±0.007	0.342±0.042	-	0.234±0.006	0.231±0.003	0.230±0.010	0.223±0.009
	192	0.388±0.011	0.326±0.009	0.350±0.010	0.225±0.012	-	-	0.354±0.012	-	0.239±0.004	0.236±0.002	0.234±0.003	0.230±0.006
	336	0.416±0.028	0.335±0.010	0.405±0.011	0.242±0.022	-	-	0.392±0.006	-	0.246±0.003	0.248±0.006	0.242±0.007	0.235±0.008
	720	0.432±0.032	0.361±0.030	0.453±0.022	0.253±0.012	-	-	0.478±0.006	-	0.263±0.001	0.264±0.006	0.248±0.010	0.236±0.009
Weather	96	0.146±0.019	0.144±0.017	0.279±0.027	0.145±0.016	0.176±0.011	0.139±0.010	0.113±0.022	0.087±0.012	0.164±0.023	0.145±0.017	0.086±0.011	0.077±0.009
	192	0.148±0.022	0.145±0.015	0.264±0.013	0.144±0.012	0.166±0.022	0.160±0.037	0.144±0.020	0.086±0.007	0.158±0.024	0.147±0.025	0.083±0.011	0.080±0.010
	336	0.152±0.032	0.146±0.011	0.283±0.021	0.149±0.023	0.168±0.014	0.170±0.027	0.138±0.033	0.098±0.002	0.162±0.006	0.160±0.012	0.093±0.010	0.086±0.005
	720	0.162±0.009	0.147±0.019	0.317±0.021	0.152±0.029	0.149±0.034	0.148±0.040	0.141±0.026	0.102±0.005	0.136±0.020	0.135±0.008	0.099±0.009	0.086±0.006
Exchange	96	0.079±0.005	0.077±0.001	0.069±0.007	0.079±0.002	0.033±0.003	0.036±0.009	0.090±0.010	0.036±0.005	0.079±0.002	0.091±0.009	0.032±0.002	0.029±0.002
	192	0.081±0.015	0.078±0.008	0.069±0.007	0.081±0.002	0.044±0.004	0.058±0.007	0.106±0.010	0.058±0.005	0.100±0.019	0.087±0.005	0.040±0.005	0.037±0.006
	336	0.086±0.003	0.083±0.005	0.071±0.005	0.085±0.010	0.074±0.017	0.058±0.009	0.106±0.010	0.076±0.006	0.086±0.008	0.091±0.002	0.054±0.001	0.050±0.002
	720	0.116±0.022	0.113±0.015	0.097±0.011	0.126±0.001	0.182±0.010	0.191±0.006	0.142±0.009	0.173±0.020	0.113±0.016	0.103±0.009	0.084±0.017	0.077±0.012
ILI	24	0.303±0.021	0.265±0.027	0.271±0.032	0.382±0.018	0.124±0.019	0.118±0.033	0.242±0.086	0.263±0.012	0.296±0.044	0.283±0.001	0.116±0.011	0.101±0.008
	36	0.262±0.013	0.222±0.047	0.258±0.058	0.286±0.037	0.144±0.011	0.143±0.089	0.246±0.117	0.298±0.011	0.298±0.048	0.307±0.007	0.142±0.008	0.134±0.009
	48	0.334±0.028	0.262±0.023	0.225±0.043	0.291±0.032	0.159±0.020	0.160±0.039	0.275±0.044	0.301±0.034	0.320±0.025	0.314±0.009	0.152±0.017	0.140±0.011
	60	0.288±0.031	0.278±0.017	0.245±0.017	0.287±0.023	0.216±0.014	0.183±0.019	0.272±0.020	0.299±0.013	0.325±0.068	0.333±0.005	0.167±0.007	0.155±0.006

C.6 Impact of Reversible Normalization (RevIN)

To verify the structural rationale of LSG-VAE, we conduct an additional ablation study focusing on the stationarity handling module (RevIN). The results are presented in Table 8.

Real-world time series data inherently exhibit non-stationary characteristics, such as time-varying means and variances (distribution shift), which challenge the generalization capability of deep generative models. To investigate the necessity of handling such shifts, we conduct an ablation by removing the RevIN module (denoted as *w/o RevIN*). As observed in Table 8, removing RevIN leads to a significant degradation in performance, particularly on datasets with strong temporal drift like *ETTh1* and *Weather*. This confirms that RevIN is indispensable for stabilizing the input distribution. By symmetrically normalizing inputs and denormalizing outputs, it allows the LSG-VAE backbone to focus on modeling local heteroscedastic dynamics rather than being distracted by global distributional shifts.

Table 8. Ablation study on Reversible Instance Normalization (RevIN) on *ETTh1* and *Weather*. We compare the full LSG-VAE (**Ours**) against the variant without RevIN (**w/o RevIN**). **Bold** indicates the best result.

Dataset	Horizon	CRPS ↓		NMAE ↓	
		w/o RevIN	Ours	w/o RevIN	Ours
ETTh1	96	0.480	0.252	0.618	0.328
	192	0.476	0.277	0.615	0.365
	336	0.470	0.300	0.603	0.384
	720	0.567	0.310	0.690	0.389
Weather	96	0.084	0.070	0.106	0.077
	192	0.097	0.067	0.125	0.080
	336	0.092	0.071	0.119	0.086
	720	0.098	0.073	0.124	0.086

C.7 Hyperparameter Sensitivity Analysis

To identify the optimal configuration and verify the robustness of LSG-VAE, we conduct a sensitivity analysis on three key hyperparameters: Patch Length (P), Hidden Dimension (D), and Number of Layers (N). We perform experiments on the representative forecasting task ($L = 96 \rightarrow H = 192$). Table 9 details the performance on two distinct datasets: *ETTh1* (representative of datasets with strong periodicity) and *Weather* (representative of high-dimensional, volatile datasets).

Table 9. **Hyperparameter Sensitivity** ($L = 96 \rightarrow H = 192$). We report CRPS on *ETTh1* and *Weather*. The default setting is updated to the optimal configuration: $P = 24, D = 256, N = 3$.

Parameter	Patch Length (P)		Hidden Dim (D)		Hidden Layers (N)	
Dataset	Value	CRPS	Value	CRPS	Value	CRPS
ETTh1	16	0.278	64	0.280	1	0.279
	24	0.277	128	0.279	2	0.278
	32	0.278	256	0.277	3	0.277
	48	0.294	512	0.278	4	0.274
Weather	16	0.069	64	0.084	1	0.074
	24	0.067	128	0.086	2	0.074
	32	0.077	256	0.067	3	0.067
	48	0.073	512	0.074	4	0.067

Analysis As detailed in Table 9, LSG-VAE demonstrates general robustness to hyperparameter variations across different domains. The performance fluctuations are relatively minor, indicating that the model does not require meticulous tuning to achieve high-quality forecasts. To strike an optimal balance between performance and computational efficiency across all datasets, we uniformly adopt the configuration of $P = 24, D = 256, N = 3$. This setting ensures sufficient model capacity and receptive field coverage while maintaining a lightweight architecture, avoiding the diminishing returns observed with larger models (e.g., $D = 512$ or $N = 4$).

C.8 Showcases

To provide a more comprehensive qualitative assessment of LSG-VAE’s modeling capabilities, we present additional visualization results on four distinct datasets: *ETTh2*, and *ETTm1*, *ETTm2*, *Weather*. These cases cover a wide spectrum of temporal dynamics, ranging from smooth periodic trends to highly volatile fluctuations and structural breaks.

Adaptive Responsiveness in Volatile Regimes Figure 7 illustrates performance on *ETTh2* and *ETTm1*, which contain complex volatility and abrupt regime shifts (e.g., the step-like drops in the top row of *ETTh2*). Here, LSG-VAE demonstrates its *adaptive attenuation* capability: its confidence intervals dynamically expand precisely when the series undergoes a sudden transition or volatility spike, and contract immediately once the series stabilizes. Baseline models, conversely, tend to generate static, uniform bands that fail to capture the temporal structure of the uncertainty. This visual evidence strongly supports our claim that the Location-Scale formulation effectively transforms the model from a passive curve fitter into an active, context-aware risk estimator.

Failure of Baselines in Stable Regimes As shown in Figure 6, specifically on the *Weather* and *ETTm2* datasets, the ground truth series exhibit high stability or smooth periodicity. In these scenarios, an ideal probabilistic model should output narrow confidence intervals (CIs) to reflect low aleatoric uncertainty. However, baseline methods—including the generative K^2 VAE and the probabilistic-enhanced point forecasters (Koopas, PatchTST)—produce excessively wide and “bloated” uncertainty bands. This phenomenon confirms that standard MSE-based or reconstruction-based objectives struggle to recognize low-volatility regimes, resulting in uninformative predictions that overestimate risk. In contrast, LSG-VAE correctly identifies the low volatility, producing sharp and tight CIs that closely hug the ground truth.

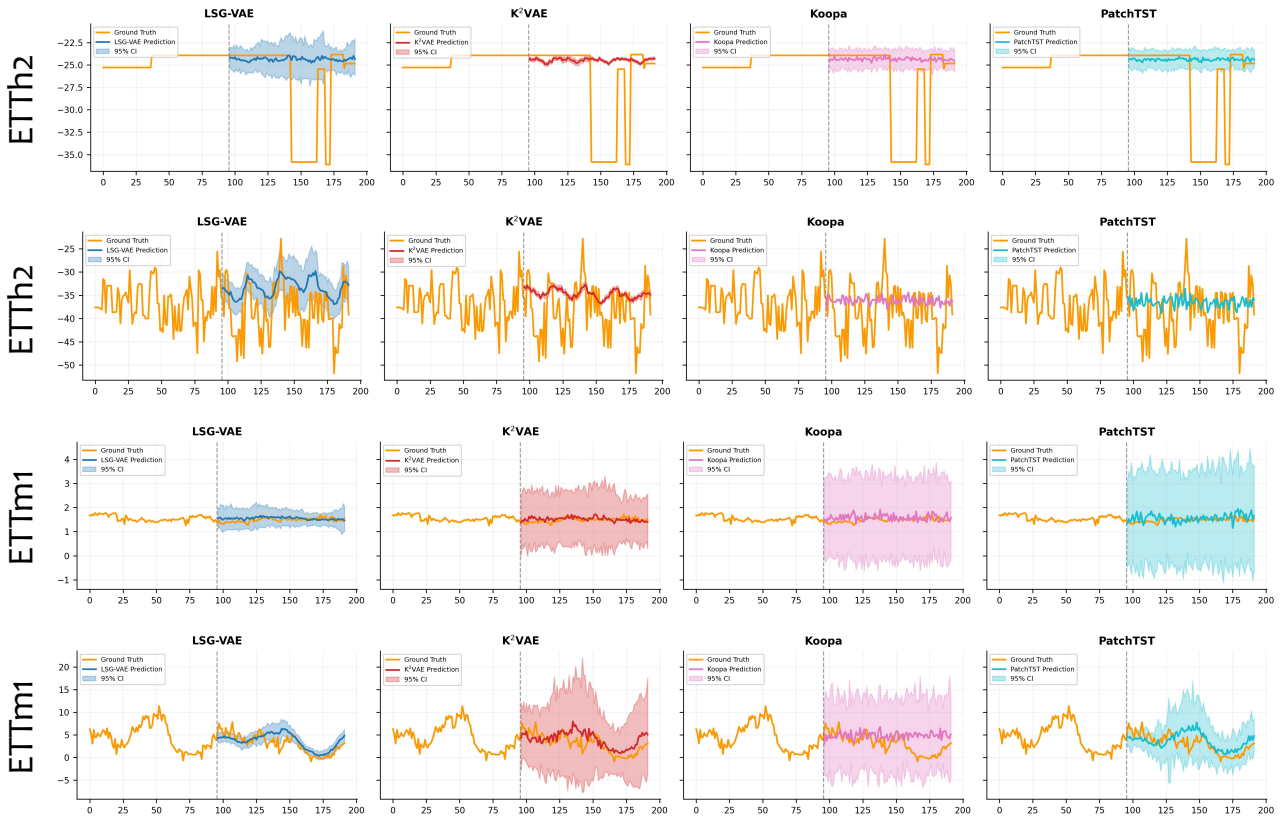


Figure 6. Visualization on Volatile Regimes (*ETTh2*, *ETTm1*). All subfigures share a unified Y-axis scale. This figure highlights performance under high volatility and structural breaks. Observation: Note the top row of *ETTh2*, where the data exhibits sudden jumps. LSG-VAE exhibits superior temporal adaptability, where its uncertainty bands expand specifically at the moments of regime shift and contract otherwise. Conversely, baselines produce static, uninformative bands that fail to capture the dynamic nature of the risk.

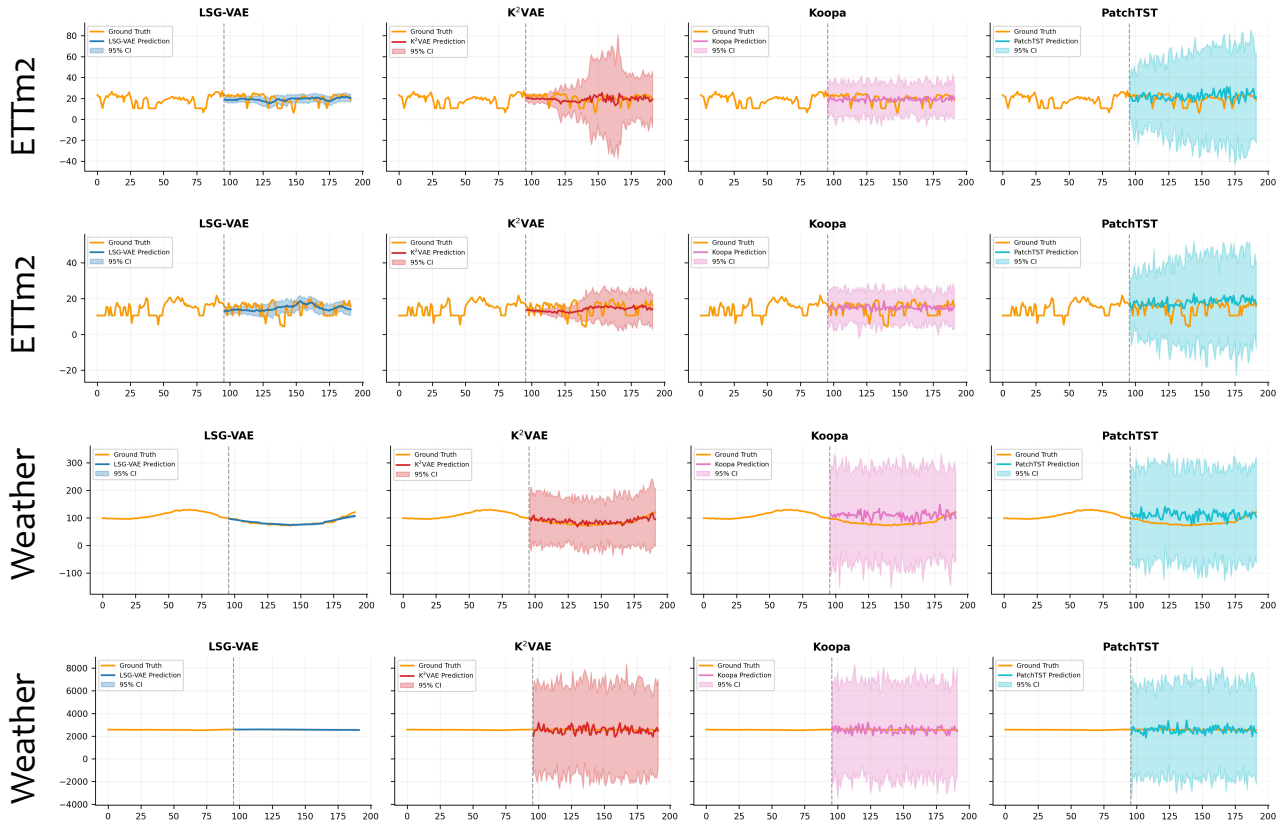


Figure 7. Visualization on Stable Regimes (*ETtm2*, *Weather*). All subfigures share a unified Y-axis scale. We compare LSG-VAE against baselines on time series with smooth trends. Observation: Baselines (K^2 VAE, Koopa, PatchTST) suffer from severe uncertainty over-estimation, generating extremely wide confidence intervals even for flat or smooth curves (e.g., *Weather*). LSG-VAE (Blue) accurately estimates the minimal aleatoric uncertainty, producing sharp and precise intervals that reflect the true high confidence of the prediction.